Climate-driven disturbances amplify forest drought sensitivity

Meng Liu[1,2], Anna T. Trugman[3], Josep Peñuelas[4,5], William R. L. Anderegg[1,2]

[1]School of Biological Sciences, University of Utah, Salt Lake City, UT, USA

[2]Wilkes Center on Climate Science and Policy, University of Utah, Salt Lake City, UT, USA

[3]Department of Geography, University of California Santa Barbara, Santa Barbara, CA, USA

[4]CREAF, Cerdanyola del Vallès, Barcelona, Catalonia, Spain

[5]CSIC, Global Ecology Unit CREAF-CSIC-UAB, Bellaterra, Barcelona, Catalonia, Spain

Corresponding author: Meng Liu (meng.liu@tamu.edu)

Abstract

Forests are a major terrestrial carbon sink, but the increasing frequency and intensity of climate-driven disturbances such as droughts, fires, and biotic agent outbreaks is threatening carbon uptake and sequestration. Determining how climate-driven disturbances may alter the capacity of forest carbon sinks in a changing climate is crucial. Here, we show that the sensitivity of gross primary productivity (GPP) to subsequent water stress increased significantly after initial drought and fire disturbances in the conterminous United States. Insect outbreak events, however, did not have significant impacts. Hot and dry environments generally exhibited increased sensitivity. Estimated ecosystem productivity and terrestrial carbon uptake decreased markedly with future warming scenarios due to the increased sensitivity to water stress. Our results highlight that intensifying disturbance regimes are likely to further impact forest sustainability and carbon sequestration, increasing potential risks to future terrestrial carbon sinks and climate change mitigation.

Main text

Terrestrial vegetation stores 450 Pg of carbon (C) and sequesters ~1.9 Pg C per year[1] (net C sink), which counterbalances approximately 20% of global C emissions from fossil fuel burning. As the primary driver of the terrestrial C sink, forests play a key role in regulating terrestrial ecosystems and the C cycle. Forests in the conterminous United States (CONUS) sequester 173 Tg C per year[2], and offset 9.7% of anthropogenic C emissions annually. Forest-based strategies to mitigate climate change, such as reforestation, improved forest management, and avoidance of forest loss, have been proposed as potentially impactful 'nature-based climate solutions' alongside dramatic reductions in fossil-fuel emissions[3,4]. However, disturbances that are sensitive to climate, such as droughts, fires, and insect outbreaks, decrease forest productivity, increase tree mortality, and decrease C storage, at least at short timescales[5–8]. At regional scales and over longer timescales, changes in disturbance regimes (e.g. more frequent and/or more severe disturbances) impair forest resistance (i.e. the capacity of the ecosystem to maintain its state and function[9]) and increase the risk of decreasing long-term C storage, which is crucial for mitigating climate change[10]. The frequency and intensity of prevalent disturbances, particularly droughts, fires, and those from biotic agents (e.g. insect outbreaks), are projected to increase in response to global warming[11–13] and will likely play a pivotal role in future forest C sink. Identifying the changes and dynamics of forest gross primary production (GPP) and how forests respond to environmental stressors after disturbances is paramount in systematically managing terrestrial ecosystems and effectively mitigating climate change.

Climate-driven disturbances have both direct and indirect effects on forest GPP. Direct effects often involve a concomitant decrease in GPP during disturbances. For example, the severe heat and drought event in 2003 led to a 30% decrease in ecosystem GPP in Europe[14], resulting in a strong anomalous net forest carbon source. However, these direct effects are typically short-lived for droughts, with forest GPP rebounding to pre-disturbance levels within a few months to a year[15]. Though, if trees die during fires and insect outbreaks, forest GPP recovery may take multiple years or longer. Indirect effects, on the other hand, refer to changes in the sensitivity of forest GPP to climate stressors after disturbances, which can persist for several years. The sensitivity of forest GPP to water stress, particularly water availability, is a critical measure of

response that indicates the "resistance" of forests to environmental variability and their capacity to sequester carbon. High sensitivity (low resistance) to water stress often signifies a high vulnerability to water deficits and climatic extremes, frequently preceding an increase in forest mortality[16]. The sensitivity of forest productivity, including GPP, tree-ring width, basal area growth, and greenness, to drought can be influenced by various factors, such as environmental conditions (soil, topography, and climate), stand composition (species and age), plant functional traits (wood density and hydraulic traits), and human management[9,17–24]. However, a comprehensive understanding of the indirect effects of disturbances on forest GPP is currently lacking. It remains unknown whether forest GPP becomes more or less sensitive to water stress after disturbances. Quantifying the long-term changes in the sensitivity of GPP to water stress in response to disturbances is crucial for enhancing our understanding and modeling the impacts of climate change on forest carbon cycling in the 21st century.

We aimed to investigate whether the sensitivity of ecosystem GPP to water stress changes after severe droughts, fires, and insect outbreaks. We examined the factors driving these changes and assessed their implications for carbon uptake. Leveraging long-term remotely sensed GPP data in CONUS, we performed regression analysis to understand the response of plant productivity to variations in water stress, as indicated by widely used drought indices like the Palmer Drought Severity Index (PDSI)[25] and the Standardized Precipitation–Evapotranspiration Index (SPEI)[26]. We calculated the sensitivity of forest GPP to water stress (referred to as "drought sensitivity") and compared it before and after disturbances. Machine learning models, specifically Random Forest regression, were employed to uncover the drivers and potential mechanisms underlying changes in drought sensitivity. We sought to answer the following research questions: 1) How does drought sensitivity change after severe disturbances across CONUS? 2) How do changes in drought sensitivity vary across different land-cover and ecosystem types? 3) What are the major factors influencing changes in drought sensitivity? 4) How might the observed changes in drought sensitivity affect vegetation carbon uptake under future warming scenarios?

Change in drought sensitivity at the continental scale

The drought sensitivity across CONUS changed significantly after severe droughts and fires. We illustrated how to calculate the change in GPP drought sensitivity with schematics (Fig. 1a and b). The sensitivity increased significantly after severe droughts and fires (Fig. 1c and d; Table S1 in Supplementary Information), where the means of the changes in sensitivity (Δk) were 3.80 ± 0.95 (mean ± standard error; p = 0.0001, GLS) and 3.83 ± 0.73 (p = 0, GLS) g C m^{-2}, respectively. Most pixels (59.12%) indicated increased sensitivity after severe droughts, but some pixels in eastern and northwestern CONUS manifested decreased sensitivity (Fig. 1c). Fewer pixels were available for analyzing the effects of fires, but the increase in sensitivity after fires was still significant (Fig. 1d), with 58.64% of the available pixels indicating increased sensitivity. The sensitivity, however, did not change significantly after insect outbreaks, −0.79 ± 1.23 (p = 0.52, GLS) g C m^{-2} (Fig. 1e). Forests in the northwest had decreased sensitivity after insect outbreaks, while Rocky Mountains had increased sensitivity. The results were similar when using SPEI to represent water stress (Extended Data Fig. 1a–c), where the sensitivity increased significantly across CONUS after severe droughts and fires, at 5.68 ± 2.06 (p = 0.0058, GLS) and 3.95 ± 1.73 (p = 0.023, GLS) g C m^{-2}, respectively, and decreased significantly after insect outbreaks, −6.22 ± 2.73 (p = 0.022, GLS) g C m^{-2}. We note as well that the patterns were robust when considering only pixels with significant GPP–PDSI relationships (Extended Data Fig. 2; Table S2). In summary, disturbances clearly altered GPP drought sensitivity, but the directions of the change in sensitivity diverged among disturbances and regions.

The sensitivity increased significantly (Δk = 6.21 ± 1.06 g C m^{-2}, p = 0, GLS; Table S3) in hot and dry regions (e.g. T > 10 °C and P < 1000 mm) (Fig. 1f) and did not change in cold and wet regions (e.g. T < 10 °C and P > 2000 mm) after severe droughts. The sensitivity increased significantly in hot and dry regions after fires (Δk = 5.33 ± 0.72 g C m^{-2}, p = 0, GLS), though there were almost no wet regions (only five pixels) (Fig. 1g), because fire was concentrated in dry regions. After insect outbreaks, the sensitivity did not change in hot and dry regions and decreased significantly in cold and wet regions (Δk = −28.49 ± 6.80 g C m^{-2}, p = 0.0002, GLS) (Fig. 1h). The intercept of the GPP–PDSI model decreased significantly after disturbances, where the means of the changes in the intercept (Δb) were all significantly lower than zero: −7.91 ± 3.51 (p

= 0.024, GLS), −7.73 ± 0.90 (p = 0, GLS), and −7.80 ± 1.94 (p = 0.0001, GLS) g C m^{-2} (Extended Data Fig. 3).

Change in drought sensitivity among land-cover types

The drought sensitivity of forests generally increased after severe disturbances, although with some notable differences among forest types. The sensitivity increased after severe droughts for evergreen needleleaf, evergreen broadleaf, and deciduous broadleaf forests (Extended Data Fig. 4, Fig. 2a, and Table S1), with the largest increase in deciduous broadleaf forests (5.47 ± 2.22 g C m^{-2}; p = 0.014, GLS). Evergreen and deciduous broadleaf forests were more sensitive to water stress after fires, and evergreen needleleaf forests were less sensitive, at −0.73 ± 0.45 g C m^{-2} (Fig. 2b). The change in the sensitivity was only significant in deciduous broadleaf forests, at 6.67 ± 3.08 (p = 0.031, GLS) g C m^{-2}. The drought sensitivity of forests did not change after insect outbreaks. The changes in the sensitivity of shrubland and grassland were large but not always significant. The changes in drought sensitivity were highly unlikely to be due to long-term trends, because undisturbed regions had different trends in sensitivity during 1982–2018 compared to disturbed regions with the same land-cover type (Extended Data Fig. 5). These results confirmed that the sensitivity of forests was affected by severe disturbances and that the sensitivity tended to increase after disturbances. The results were comparable when using SPEI (Extended Data Fig. 1d–f), where evergreen broadleaf and deciduous broadleaf forests exhibited significantly increased sensitivity, at 23.50 ± 8.14 (p = 0.0041, GLS) and 16.18 ± 7.04 (p = 0.022, GLS) g C m^{-2}, after severe droughts.

The intercept of the GPP–PDSI model decreased in forests (Fig. 2 and Table S1). The decreases were due to lower biomass and foliar area caused by disturbances, leading to decreased forest productivity. The directions of the changes in the intercept were not consistent for grassland and shrubland. It is very intriguing that the intercept of shrubland increased after all three disturbances, which might indicate that the direct effects (GPP decrease) of disturbances on shrubland can recover quickly. However, the intercept change is not strictly related to the absolute GPP change since we used detrended GPP. From the perspective of vegetation structure, shrubs have smaller leaf area, frequent resprouting behaviors, and shorter canopy heights than forests, which might benefit the recovery of shrubland productivity after disturbances.

Factors influencing the change in drought sensitivity

Several climatic factors play a crucial role in driving the change in drought sensitivity. These factors include the trend of soil moisture (Trend.SM), mean annual temperature (MAT), the interaction between temperature and reversed precipitation (Interaction.TP), and downward surface shortwave radiation (Srad). For drought, the Random Forest model explained 67% of the variation (R^2 = 0.67; Extended Data Fig. 6a) in the change in sensitivity, with the trend of soil moisture emerging as the most important driver (Fig. 3a). Mean annual temperature and the interaction between temperature and reversed precipitation ranked as the second and third most important drivers, respectively. The change in sensitivity increased with decreasing trends of soil moisture (Fig. 3b), indicating that lower soil moisture levels contributed to higher post-disturbance sensitivity. Similarly, the change in sensitivity increased with mean annual temperature (Fig. 3c), suggesting that regions experiencing higher temperatures were more likely to exhibit increased sensitivity after disturbances. The interaction between temperature and reversed precipitation (Fig. 3d) had similar effects to mean annual temperature, with higher values (indicating hot and dry regions) associated with increased drought sensitivity.

For fires and insect outbreaks, the Random Forest models explained 37% and 28% of the variations in sensitivity change, respectively (Extended Data Fig. 6b and c). Mean annual temperature emerged as the most important driver for fires (Fig. 3e), where regions with higher temperatures were associated with increases in sensitivity after the disturbance (Fig. 3f), particularly when mean annual temperature exceeded approximately 15°C. Additionally, increasing downward surface shortwave radiation (particularly when the trend of Srad is greater than zero) and a high PDSI were linked to an increase in sensitivity after fires. In the case of insect outbreaks, mean annual downward surface shortwave radiation emerged as the most important driver (Fig. 3i), with regions experiencing high radiation (e.g. > 180 W m^{-2}) demonstrating increased sensitivity, while regions with low radiation exhibited decreased sensitivity after the disturbance (Fig. 3j). This result aligns with the distribution of sensitivity change after insect outbreaks (Fig. 1e), where northwest regions generally displayed decreased sensitivity and low levels of shortwave radiation. Increasing trends in CO_2 and shortwave radiation also contributed to the increase in sensitivity after insect outbreaks (Fig. 3k and l).

Impacts on C uptake

The change in drought sensitivity of GPP has notable implications for C uptake and loss. We quantified C uptake responses to water stress and assessed the recovery time by utilizing pixels with a post-disturbance period of at least 16 years (see Methods). It took approximately five years for the sensitivity to return to the pre-disturbance level after severe droughts and around six years after fires (Extended Data Fig. 7b and c). Due to the relatively short post-disturbance time (nine years: 2010–2018), the recovery time for insect outbreaks was not calculated. We further estimated the potential change in C uptake resulting from the sensitivity change. As a first-order exploration, the change in C uptake was calculated as the difference in GPP when considering the changes in sensitivity and intercept (equation (2)). For drought, the mean annual change in C uptake over the five-year period following the disturbance was −9.94 ± 2.99 Tg C (Fig. 4a) across CONUS, indicating a reduction in C absorption. For fires, the mean annual change in C uptake over the six-year period after the disturbance was −1.50 ± 0.03 Tg C (Fig. 4c). To assess the effects of future warming, PDSI under +2 °C warming scenario was used to estimate the change in C uptake in response to the sensitivity change. For drought, the change in C uptake under the +2 °C warming scenario was estimated to be −11.21 ± 2.42 Tg C (Fig. 4b), indicating even lower C absorption than historical conditions. For fires, the change in C uptake was estimated to be −1.63 ± 0.04 Tg C under the warming scenario (Fig. 4d).

Implications for climate change mitigation

Severe disturbances, such as severe droughts, fires, and insect outbreaks, have significant impacts on forest ecosystems. They all have the potential to alter forest composition, leading to a shift towards early succession species[27], and can cause physiological damage to surviving trees. Both effects influence the sensitivity of post-disturbance forest productivity to water availability. This study specifically examines the indirect effects of severe disturbances and highlights the changes in GPP drought sensitivity following these extreme events. We have observed that severe disturbances, such as severe droughts and fires, tend to increase the sensitivity of forest productivity to water availability. This is particularly notable in deciduous broadleaf forests, possibly due to drought legacy effects[28] and disturbance-induced damage, such as embolism and overheating. These factors make trees more susceptible to subsequent water stress. Additionally,

for deciduous trees, physiological traits such as shallow roots[29] and thin bark likely contribute to increased susceptibility to fire and drought damage. In contrast, for evergreen needleleaf forests, the sensitivity did not change and even decreased after fires and insect outbreaks. This phenomenon may be attributed to decreases in stand density following disturbances. Generally, stand density has increased in many evergreen needleleaf forests in the western United States due to historical fire suppression activities[30]. Disturbances can relax overstocked conditions and reduce competition[31] for water. This result suggests that thinning holds the potential to alleviate water stress in certain conifer forests. Additionally, gymnosperm-dominated forests, mainly needleleaf forests in the western United States, have shown notable shifts characterized by decreases in P50 (water potential at which 50% of conductivity is lost) and increases in HSM (hydraulic safety margin, the difference between P50 and the minimum water potential experienced)[32] in response to climate-driven mortality, making these forests more drought-tolerant.

Non-forested ecosystems, such as shrublands and grasslands, also exhibit heightened drought sensitivity following disturbances, especially after severe droughts and fires. This increased sensitivity may be attributed to their proximity to absolute biogeographic and climate thresholds. Shrubs and grasses predominantly thrive in arid regions characterized by high solar radiation and temperature coupled with low water availability. Moreover, dry regions, particularly shrublands and grasslands, reveal stronger correlations between GPP and PDSI (Extended Data Fig. 2b). Climate emerges as a crucial factor influencing sensitivity changes, with hot and dry regions experiencing increased sensitivity and cold and wet regions showing decreased sensitivity (Fig. 1). Previous research[28] also indicates that plants in arid regions exhibit stronger drought legacy effects compared to those in wet regions.

Droughts, fires, and insect outbreaks have varied impacts on ecosystems. In general, understory species such as grasses and herbs are sensitive to water availability[33] and usually senesce rapidly due to water deficits. During droughts, both the understory and overstory vegetation will be constrained. The absolute GPP values of understory grasses might recover in the next year; however, the GPP sensitivity to water (i.e. indirect effects) of the whole ecosystem, including both the understory and overstory vegetation, may not recover as quickly. The

sensitivity of grasslands increased significantly (p = 0, GLS) after droughts (Fig. 2a), indicating that the GPP sensitivity of grasses may not necessarily recover at the same pace as the absolute GPP. For overstory trees, drought legacy effects can last for years[28]. A similar situation goes for fires, where both the understory grasses and overstory trees might be burned during fires. The absolute GPP of understory grasses can recover quickly; however, the GPP sensitivity might not (Fig. 2b). For overstory trees, fire damage, such as heat stress (e.g. heat emboli) and biomass consumption, can cause a long-lasting sensitivity change. For insect outbreaks, understory grasses are not the target of widespread insects like bark beetles[7], and thus the impacts of insects on understory vegetation will be small. The unchanged (or even decreased) sensitivity after insect outbreaks could be due to the decreases in stand density and shifts in composition.

Across CONUS, the increased sensitivity of GPP to water stress leads to substantial decreases in C uptake after severe droughts and fires. These decreases are logical as photosynthesis and C uptake tend to decline more when sensitivity increases at the same level of water stress, and climate change is likely to bring more frequent and severe droughts in many regions. Our estimates suggest that the decrease in C uptake can persist for approximately 5~6 years after the disturbances. This reduction in C uptake hampers the capacity of terrestrial ecosystems to sequester anthropogenic C emissions. Furthermore, our findings highlight the accelerated decline in C uptake under warming scenarios. Less carbon would be absorbed in response to increased sensitivity under warming scenarios compared to historical conditions. Many regions in CONUS are projected to experience hotter and drier conditions under future warming scenarios[13], leading to increased water stress on plant growth. As a result, ecosystems' ability to absorb carbon would decline, exacerbated by increased water stress and vegetation sensitivity. Regions such as western North America face high risks of carbon loss and species loss due to climate change, as indicated by global assessments[34].

Climate change is expected to increase the frequency and severity of disturbances in many regions. From the perspective of climate policy and management, relying on planting more trees to counterbalance C emissions from fossil fuel burning can be challenging, particularly when ecosystem productivity is threatened by disturbances that are climate dependent. Our results highlight pervasive changes in the drought sensitivity of GPP in forests after disturbances and

imply meaningful impacts on C uptake. Increased sensitivity increases the vulnerability of ecosystems to drought and could lead to substantial decreases in ecosystem C uptake under future warming scenarios. These long-term dynamics are important for evaluating the capacity of terrestrial ecosystems as C sinks for C management, nature-based climate solutions, and net-zero pledges.

Acknowledgements

The study was supported by the Wilkes Center at the University of Utah, and thanks to the Anderegg lab. J.P. was supported by the TED2021-132627B-I00 grant, funded by MCIN and the European Union NextGeneration EU/PRTR, and the CIVP20A6621 grant funded by the Fundación Ramón Areces. A.T.T. acknowledges funding from National Science Foundation Grants 2003205, 2017949 and 2216855, the University of California Laboratory Fees Research Program Award No. LFR-20-652467, and the Gordon and Betty Moore Foundation Grant GBMF11974. W.R.L.A. acknowledges support from the David and Lucille Packard Foundation and US National Science Foundation grants 1802880, 2003017 and 2044937.

Author Contributions Statement

M.L. and W.R.L.A. conceptualized and designed the study with input from all co-authors. M.L. performed the analysis. M.L. wrote the initial draft and A.T.T., J.P. and W.R.L.A. discussed the design, analyses and results and provided extensive and valuable comments and revisions.

Competing Interests Statement

The authors declare no competing interests.

Figure Legends/Captions

Fig. 1 The sensitivity of vegetation to water stress in CONUS changed significantly after severe disturbances. (**a**–**b**) Schematics of (**a**) GPP anomalies (detrended) and PDSI, and (**b**) change in sensitivity due to disturbances. (**c**–**e**) The change in sensitivity after severe (**c**) droughts, (**d**) fires, and (**e**) insect outbreaks. Asterisks indicate significance at the 0.05 level (two-sided) based on the generalized least squares (GLS) model. Multiple comparisons are not applicable. The distribution maps (4 km) for fires and insect outbreaks were aggregated to 20 km for visual

display. (**f**–**h**) The change in sensitivity in climate space (mean annual temperature (MAT) vs mean annual precipitation (MAP); 1 °C ×100 mm grid).

Fig. 2 The drought sensitivity of forests increased after severe disturbances. The mean changes in sensitivity (Δ*k*) and intercept (Δ*b*) for different land covers in CONUS after severe (**a**) droughts (left to right, *N*=2401, 414, 4691, 1127, 7719), (**b**) fires (*N*=1944, 178, 258, 601, 6068), and (**c**) insect outbreaks (*N*=7320, 111, 548, 157, 3904). The error bars are standard errors, and the asterisks indicate that the mean is significant at the 0.05 level (two-sided) based on the GLS model. Multiple comparisons are not applicable. ENF, evergreen needleleaf forest; EBF, evergreen broadleaf forest; DBF, deciduous broadleaf forest.

Fig. 3 Drivers of the change in GPP drought sensitivity. (**a**–**d**) Drivers of the change in the sensitivity of GPP to water stress after severe droughts: (**a**) importance of drivers and (**b**–**d**) Random Forest partial dependence of the change in sensitivity on the three most important drivers. (**e**–**h**) Drivers of the change in the sensitivity of GPP to water stress after severe fires. (**i**–**j**) Drivers of the change in the sensitivity of GPP to water stress after severe insect outbreaks. The solid black line is the average, and the shading shows the range (i.e. from minimum to maximum) of the partial dependence from 100 runs of Random Forest models.

Fig. 4 Carbon (C) uptake decreases in warming scenarios. (**a**–**b**) The average change in C uptake (ΔC) due to the change in sensitivity after severe droughts under (**a**) historical time and (**b**) +2 °C warming scenario. (**c**–**d**) The average ΔC due to the change in sensitivity after severe fires. 'Annual' indicates mean annual total ΔC across CONUS, and the asterisk indicates the mean is significant at the 0.05 level (two-sided, both GLS models and t test). Multiple comparisons are not applicable. Panels **c**–**d** are aggregated to 20 km for visual display.

References

1. Friedlingstein, P. *et al.* Global Carbon Budget 2022. *Earth System Science Data* **14**, 4811–4900 (2022).
2. Wear, D. N. & Coulston, J. W. From sink to source: Regional variation in U.S. forest carbon futures. *Sci Rep* **5**, 16518 (2015).
3. Griscom, B. W. *et al.* Natural climate solutions. *PNAS* **114**, 11645–11650 (2017).

4. Fargione, J. E. *et al.* Natural climate solutions for the United States. *Science Advances* **4**, eaat1869 (2018).
5. Seidl, R. *et al.* Forest disturbances under climate change. *Nature Clim Change* **7**, 395–402 (2017).
6. McDowell, N. G. & Allen, C. D. Darcy's law predicts widespread forest mortality under climate warming. *Nature Clim Change* **5**, 669–672 (2015).
7. Williams, C. A., Gu, H., MacLean, R., Masek, J. G. & Collatz, G. J. Disturbance and the carbon balance of US forests: A quantitative review of impacts from harvests, fires, insects, and droughts. *Global and Planetary Change* **143**, 66–80 (2016).
8. Hemes, K. S., Norlen, C. A., Wang, J. A., Goulden, M. L. & Field, C. B. The magnitude and pace of photosynthetic recovery after wildfire in California ecosystems. *Proceedings of the National Academy of Sciences* **120**, e2201954120 (2023).
9. Anderegg, W. R. L., Trugman, A. T., Badgley, G., Konings, A. G. & Shaw, J. Divergent forest sensitivity to repeated extreme droughts. *Nat. Clim. Chang.* **10**, 1091–1095 (2020).
10. Anderegg, W. R. L. *et al.* Climate-driven risks to the climate mitigation potential of forests. *Science* **368**, eaaz7005 (2020).
11. Anderegg, W. R. L. *et al.* Future climate risks from stress, insects and fire across US forests. *Ecology Letters* **25**, 1510–1520 (2022).
12. Dai, A. Drought under global warming: a review. *WIREs Climate Change* **2**, 45–65 (2011).
13. Cook, B. I., Ault, T. R. & Smerdon, J. E. Unprecedented 21st century drought risk in the American Southwest and Central Plains. *Science Advances* **1**, e1400082 (2015).
14. Ciais, P. *et al.* Europe-wide reduction in primary productivity caused by the heat and drought in 2003. *Nature* **437**, 529–533 (2005).
15. Schwalm, C. R. *et al.* Global patterns of drought recovery. *Nature* **548**, 202–205 (2017).
16. Keen, R. M. *et al.* Changes in tree drought sensitivity provided early warning signals to the California drought and forest mortality event. *Global Change Biology* **28**, 1119–1132 (2022).
17. Fu, Z. *et al.* Sensitivity of gross primary productivity to climatic drivers during the summer drought of 2018 in Europe. *Philosophical Transactions of the Royal Society B: Biological Sciences* **375**, 20190747 (2020).

18. Phillips, R. P. *et al.* A belowground perspective on the drought sensitivity of forests: Towards improved understanding and simulation. *Forest Ecology and Management* **380**, 309–320 (2016).
19. McDowell, N. *et al.* Mechanisms of plant survival and mortality during drought: why do some plants survive while others succumb to drought? *New Phytologist* **178**, 719–739 (2008).
20. Cartwright, J. M., Littlefield, C. E., Michalak, J. L., Lawler, J. J. & Dobrowski, S. Z. Topographic, soil, and climate drivers of drought sensitivity in forests and shrublands of the Pacific Northwest, USA. *Sci Rep* **10**, 18486 (2020).
21. Rosner, S. *et al.* Wood density as a screening trait for drought sensitivity in Norway spruce. *Can. J. For. Res.* **44**, 154–161 (2014).
22. Mausolf, K. *et al.* Higher drought sensitivity of radial growth of European beech in managed than in unmanaged forests. *Science of The Total Environment* **642**, 1201–1208 (2018).
23. Lebourgeois, F., Gomez, N., Pinto, P. & Mérian, P. Mixed stands reduce Abies alba tree-ring sensitivity to summer drought in the Vosges mountains, western Europe. *Forest Ecology and Management* **303**, 61–71 (2013).
24. Linares, J. C., Taïqui, L., Sangüesa-Barreda, G., Seco, J. I. & Camarero, J. J. Age-related drought sensitivity of Atlas cedar (Cedrus atlantica) in the Moroccan Middle Atlas forests. *Dendrochronologia* **31**, 88–96 (2013).
25. Palmer, W. C. Meteorological drought. *U.s.department of Commerce Weather Bureau* (1965).
26. Beguería, S., Vicente-Serrano, S. M., Reig, F. & Latorre, B. Standardized precipitation evapotranspiration index (SPEI) revisited: parameter fitting, evapotranspiration models, tools, datasets and drought monitoring. *International Journal of Climatology* **34**, 3001–3023 (2014).
27. Trugman, A. T., Medvigy, D., Anderegg, W. R. L. & Pacala, S. W. Differential declines in Alaskan boreal forest vitality related to climate and competition. *Global Change Biology* **24**, 1097–1107 (2018).
28. Anderegg, W. R. L. *et al.* Pervasive drought legacies in forest ecosystems and their implications for carbon cycle models. *Science* **349**, 528–532 (2015).

29. Tumber-Dávila, S. J., Schenk, H. J., Du, E. & Jackson, R. B. Plant sizes and shapes above and belowground and their interactions with climate. *New Phytologist* **235**, 1032–1056 (2022).
30. Voelker, S. L. *et al.* Fire deficits have increased drought sensitivity in dry conifer forests: Fire frequency and tree-ring carbon isotope evidence from Central Oregon. *Global Change Biology* **25**, 1247–1262 (2019).
31. Sheil, D. Disturbance and distributions: avoiding exclusion in a warming world. *Ecology and Society* **21**, (2016).
32. Trugman, A. T., Anderegg, L. D. L., Shaw, J. D. & Anderegg, W. R. L. Trait velocities reveal that mortality has driven widespread coordinated shifts in forest hydraulic trait composition. *Proceedings of the National Academy of Sciences* **117**, 8532–8538 (2020).
33. Adhikari, A. *et al.* Management and climate variability effects on understory productivity of forest and savanna ecosystems in Oklahoma, USA. *Ecosphere* **12**, e03576 (2021).
34. Anderegg, W. R. L. *et al.* A climate risk analysis of Earth's forests in the 21st century. *Science* **377**, 1099–1103 (2022).

Methods

Data

We used gross primary production (GPP) to indicate the photosynthetic capacity and productivity of forests. Four state-of-the-art long-term GPP datasets covering CONUS were used: the Numerical Terradynamic Simulation Group (NTSG) Landsat GPP data set[35], the Global LAnd Surface Satellite (GLASS) GPP data set[36], the revised Eddy Covariance-Light Use Efficiency (EC-LUE) model derived GPP data set[37], and the near-infrared reflectance of vegetation (NIRv) based GPP data set[38]. The NTSG GPP data set (1986–2021) provided 16-day 30-m GPP data based on Landsat data and climatic variables across CONUS. (See Supplementary Information for details on these GPP products.) The four sets of GPP data were resampled to 4 km and aggregated to the annual level. Anomalies were calculated and detrended for each pixel for each GPP product. The four detrended anomalies were averaged for each pixel for all subsequent analysis to avoid inconsistencies and biases among the GPP products. The following analysis was based on the average anomalies of the four GPP products from 1982 to 2018.

We utilized two widely recognized drought indices, namely the Palmer Drought Severity Index (PDSI)[25,39] and the Standardized Precipitation–Evapotranspiration Index (SPEI)[26], to quantify water stress and calculate changes in GPP drought sensitivity. The PDSI is a standardized metric derived from a two-layer soil water balance model, where negative values indicate dry conditions and positive values indicate wet conditions. We obtained monthly historical PDSI data at a 4-km resolution covering the period between 1982 and 2018 from TerraClimate[40], which provides climatic variables such as temperature (T), precipitation (P), soil moisture (SM), potential evapotranspiration (PET), and downward surface shortwave radiation (Srad). The PDSI data from TerraClimate were based on the Penman–Monteith equation-based PET. Monthly PDSI values were averaged to generate annual PDSI data. Severe drought disturbances were defined as annual PDSI values below -3[25,41]. Other thresholds such as -2 and -4 were also tested, and the results were comparable when using -3 and -4. -2 usually indicates moderate droughts, which have limited effects on ecosystems. The SPEI is a multi-scalar drought index that captures atmospheric water deficits by considering the difference between precipitation and PET. In our analysis, we used monthly precipitation and PET data from TerraClimate at a 4-km resolution to

calculate the monthly 4-km SPEI12 (scale = 12-month) between 1982 and 2018 using the "SPEI" package in R. SPEI12 was selected as we used annual data in this study. Monthly SPEI12 values were averaged to the annual level, and severe droughts were defined as SPEI12 values below -1.2[9]. Other thresholds such as -1 and -1.5 were also tried, and the results were comparable when using -1.2 and -1.5. -1 is usually related to moderate droughts, which have limited impacts on ecosystems.

Maps of annual fire severity were obtained from the Monitoring Trends in Burn Severity (MTBS) database, which has provided fire maps for the United States since 1984. The 30-m resolution maps of annual fire severity between 1984 and 2018 were downloaded and aggregated to 4 km. Low-severity pixels were discarded because low-severity fires generally have very small impacts on forests. The proportion of burned 30-m pixels (moderate- and high-severity pixels) within each 4-km grid was calculated when aggregating the 30-m pixels to 4-km data. A 4-km grid was treated as burned when the proportion was > 10%. Plots from the Forest Inventory and Analysis (FIA) program were used to identify damage caused by insect outbreaks. Agent Codes (AGENTCD) of 10–19 for the FIA plots indicates that insects caused mortality. The rates of mortality of basal area due to insects were used to indicate insect damage. The mean annual rate of mortality for each plot during 2000–2009 was taken from Anderegg et al. (2022)[11]. We aggregated the plots to 4 km and calculated the average rate for each pixel. An average rate > 0.3% was used to define insect outbreaks. The species of biotic agents (particularly insects here) were not provided by the FIA data.

Land-cover maps at a resolution of 500 m from the Terra and Aqua combined MODIS Land Cover Type (MCD12Q1) Version 6 from 2001 to 2020 were used to identify different vegetation types. Land-cover type 5 was used, where croplands and non-vegetation (water, urban, and barren) classes were removed. Pixels with changes in land cover in 2001–2020 were also removed. We aggregated the 500-m land-cover maps to 4 km to match the GPP data. The land-cover map for 2001 is shown in Extended Data Fig. 4.

Analysis of sensitivity

The slope of a linear regression (GPP anomaly vs PDSI) was used to represent the sensitivity of photosynthesis to water availability because most pixels (~70%) in CONUS presented a linear relationship between GPP anomaly and PDSI (Extended Data Fig. 2). Those pixels presenting non-linear relationships were dominated by grasslands. Thus, while a minority of areas do not have linear GPP–PDSI relationships, our results are robust to including only significant linear relationship pixels (Extended Data Fig. 2d–f and Table S2) and a linear model represents the most parsimonious, comparable, and understandable model of drought sensitivity and thus we used it for all analyses. We compared simple linear regression and multiple linear regression when deriving the sensitivity of GPP to water stress, where the sensitivity from the two models was significantly correlated (Extended Data Fig. 8). For droughts, the slope of the linear regression between pre-drought GPP anomalies and PDSI was calculated to indicate pre-drought sensitivity (k_0). Similarly, post-drought sensitivity (k_1) was calculated using post-drought GPP anomalies and PDSI. The difference between the post-drought and pre-drought slopes was treated as the change in sensitivity (Δk).

$$\begin{cases} \text{GPP anomaly}_{\text{pre}} = k_0 \times \text{PDSI}_{\text{pre}} + b_0 \\ \text{GPP anomaly}_{\text{post}} = k_1 \times \text{PDSI}_{\text{post}} + b_1 \\ \Delta k = k_1 - k_0,\ \Delta b = b_1 - b_0 \end{cases} \quad (1)$$

where b_0 and b_1 are intercepts. The change in sensitivity derived with SPEI12 was calculated in the same way shown in equation (1), where SPEI12 was used to indicate water stress.

We required at least eight years of data for regression when calculating the slopes. Based on the histogram of drought return intervals in Extended Data Fig. 9a, eight was the first break point for drought return intervals, and the disturbance return intervals of most pixels are higher than eight years. We also tried six (the trough) and ten (the second break point) years as the minimum for regression, and the corresponding changes in sensitivity were shown in Extended Data Fig. 9c and d, respectively, which were comparable to the change in sensitivity (Δk) in Fig. 2a. Eight years strikes a reasonable balance between sample size and stability. A lower threshold, such as six years, could make the results of linear regression unstable, whereas a higher threshold would decrease the sample size. For fire (Extended Data Fig. 9b), the return intervals of most

pixels were greater than ten years, indicating that any values lower than or equal to ten were acceptable. Therefore, using eight as the minimum number of years for regression was reasonable. The length of pre-disturbance and post-disturbance data could vary, and eight years was the minimum we used for regression analysis. The first drought was checked for each pixel. The change in sensitivity was calculated when we had at least eight data points for a regression analysis before and after the first drought. Otherwise, the second drought would be checked. This pixel was discarded if all droughts were not qualified for calculating the change in sensitivity. Continuous droughts were treated as one drought when calculating the change in sensitivity. When there were two or more drought events suitable for calculating Δk, the first one would be used. The same procedure was applied to fires, producing the change in sensitivity after a fire. For insect outbreaks, we calculated the slope between GPP anomalies and PDSI before 2000 to represent pre-outbreak sensitivity, and the slope after 2009 was treated as the post-outbreak sensitivity. We resorted to this approximation due to the limited availability of standardized FIA plots, which were only accessible from 2000 onwards and repeated every five or ten years. While the strategy employed to calculate the change in sensitivity for insect outbreaks may not be ideal, it was a reasonable approach given the data constraints. To validate our findings, we conducted a sensitivity analysis by separately analyzing the four GPP anomalies and the PDSI data. The results (Extended Data Fig. 10) were comparable to those obtained using the average anomalies of the four GPP products. The sensitivity change of each land-cover type based on a single GPP product was presented in Table S4.

To account for spatial autocorrelations in the changes in sensitivity (Δk) and intercept (Δb), we employed the generalized least squares (GLS) model[42] and examined their significance. We utilized the gls function from the "nlme" package in R. The exponential correlation structure, corExp, was selected to assess the significance of the mean Δk and mean Δb by fitting GLS models with the formulas "$\Delta k \sim 1$" and "$\Delta b \sim 1$" (regression with only the constant term), respectively. We experimented with five correlation structures: exponential, sphere, gaussian, ratio, and linear. The exponential correlation structure was always ranked in the top two correlation structures for minimizing AIC. So, to save time for computation (GLS models are extremely time-consuming when dealing with large samples), we decided to use the exponential correlation structure

494 throughout the manuscript. Due to computational intensity, we aggregated the Δ*k* and Δ*b* maps
495 for drought disturbances using a factor of three (4 km to 12 km) during the calculation. If the *p*-
496 value (two-sided) was below 0.05 based on the GLS, the constant term (i.e. mean Δ*k* or mean Δ*b*)
497 was considered significant.

498 **Random Forest model**

499 We employed Random Forest regression[43], a widely-used machine learning model, to
500 capture the change in sensitivity (equation (1)) and identify the primary drivers responsible for
501 this change. Random Forest regression, which utilizes an ensemble of decision trees, is well-
502 suited for analyzing high-dimensional data, such as large sample sizes with numerous predictors
503 and complex structure. To train the Random Forest model, we utilized the "randomForest"
504 package in R. The response variable was the change in sensitivity (Δ*k*), and the predictors included
505 various variables, namely temperature (T), precipitation (P), soil moisture (SM), downward
506 surface shortwave radiation (Srad), PDSI, leaf area index (LAI)[44], and CO_2 concentration[45]. For
507 each pixel, we calculated the long-term mean (e.g. mean annual temperature) and trend (e.g. the
508 trend of temperature, which is the slope of linear regression between T and year) of these
509 variables using data from 1982 to 2018. Additionally, we incorporated the interaction between T
510 and P (Interaction.TP) as a predictor, which represented the mean quantiles of T and reversed P.
511 First, we calculated the quantiles (0–1) of T, and high T had high quantiles. Second, we reversed
512 P by multiplying −1 (i.e. −1×P) and calculated the quantiles of the reversed P. Finally, we averaged
513 the quantiles of T and reversed P. The average quantiles can represent the interaction between
514 T and P, where high quantiles imply hot and dry conditions. GPP anomalies in the disturbed years
515 and land-cover types were also included as extra predictors. Prior to training the models, highly
516 correlated predictors were removed. For instance, when mean annual precipitation and mean
517 annual soil moisture exhibited a high correlation ($|r| > 0.7$), the predictor with a lower correlation
518 with Δ*k* was eliminated. In the Random Forest models, we used 500 decision trees, and the
519 number of splits was determined as the square root of the number of selected predictors ($\lfloor\sqrt{n}\rfloor$).
520 The LAI data were obtained from the half-month 8-km Global Inventory Modeling and Mapping
521 Studies (GIMMS) LAI4g product (1982–2020)[44], which were resampled (bilinear) to 4 km and
522 averaged to the annual level. Similarly, the global monthly 1° historical CO_2 concentration data[45]

from 1982 to 2013 were resampled (bilinear) to 4 km and averaged to the annual level. Separate Random Forest models were developed for each of the three disturbances, as the drivers varied among them. The resulting partial dependence plots generated by the Random Forest models illustrated the relationships between Δ*k* and the predictors. Predictor importance was assessed based on the decrease in node purity, where the importance of a predictor was calculated as the decrease in node purity attributed to that predictor divided by the sum of the decrease in node purity for all predictors, multiplied by 100%. We ran the Random Forest models 100 times and averaged the responses (i.e. importance and partial dependence) of the 100 models (Fig. 3).

Recovery time and C uptake change

Recovery time was determined as the duration required for the sensitivity to return to its pre-disturbance level. Since the sensitivity could increase following disturbances, ecosystems may take years to recover their original states. To derive the recovery time, we selected pixels with a post-disturbance time of at least 16 years, ensuring a minimum of two independent eight-year periods to calculate sensitivity. A moving window strategy, utilizing eight-year intervals, was employed to compute post-disturbance sensitivity for each selected pixel. Within each moving window (1–8 years, 2–9 years, 3–10 years, etc.), the sensitivity was determined as the slope of linear regression between GPP anomaly and PDSI. We considered ecosystems to have recovered when the post-disturbance sensitivity was equal to or lower than the pre-disturbance sensitivity (k_0). The recovery time was defined as the first year of the moving window when the post-disturbance sensitivity was ≤ k_0. The calculation of recovery time is illustrated in the schematic provided in Extended Data Fig. 7a, which exemplifies a recovery time of 5 years. If the sensitivity decreased after disturbances, the recovery time would be identified when the post-disturbance sensitivity was ≥ k_0. The average recovery times for severe droughts and fires were 4.8 and 5.6 years, respectively. However, the recovery time for insect outbreaks could not be determined due to the limited post-disturbance period of nine years (2010–2018).

The change in carbon (C) uptake was estimated based on the change in GPP. The equation below represents the change in GPP (ΔGPP) in response to the change in sensitivity after disturbances:

$$\Delta \mathrm{GPP} = \Delta k \times \mathrm{PDSI} + \Delta b \quad (2)$$

where ΔGPP indicates the change in productivity, and Δ*k* and Δ*b* represent the changes in sensitivity and intercept, respectively (as shown in Fig. 1 and Extended Data Fig. 3). Historical PDSI data after disturbances were used to derive the change in C uptake (ΔC = ΔGPP). For severe droughts, the closest integer to 4.8 (i.e. 5 years) was employed, while for severe fires, the closest integer to 5.6 (i.e. 6 years) was used. Each pixel was associated with five PDSI values after severe droughts and six PDSI values after severe fires, which were inputted into equation (2) to calculate the corresponding ΔC. For instance, if a severe drought occurred in the tenth year, PDSI values in the eleventh, twelfth, thirteenth, fourteenth, and fifteenth years would be used in equation (2), producing five ΔGPP values. The mean annual ΔC per pixel after severe droughts and fires is presented in Fig. 4a and d, respectively, indicating a reduction in C assimilation through photosynthesis due to disturbances.

In warming scenarios, we utilized 4-km monthly precipitation and PET data under +2 °C warming obtained from Qin et al. (2020)[46] to generate PDSI values under the +2 °C scenario with the "scPDSI" package in R. The precipitation and PET data under the +2 °C scenario corresponded to the nominal years of 1985–2015. Monthly PDSI values under the warming scenario were calculated and averaged to the annual level. The change in C uptake was estimated using the annual PDSI values under the warming scenario following the same approach outlined in equation (2), with Δ*k* and Δ*b* obtained from Fig. 1 and Extended Data Fig. 3, respectively. The mean annual ΔC under the warming scenario is depicted in Fig. 4.

Caveats

The GPP products used in this study are based on different inputs and models, leading to inherent differences in results when comparing across different GPP datasets. To increase the robustness of our analysis, we used a detrended, ensemble mean approach when deriving GPP for our study. Though we believe that taking an ensemble mean strengthens the analysis above any based on a single product along, caution should be exercised in interpretation remote sensing based GPP data, which tend to overestimate vegetation productivity in droughts (particularly severe droughts[47]). To overcome the drought limitation in this study, we used pre-drought and

post-drought GPP data to conduct regression analysis, rather than data during drought. This approach avoids the potential limitations of GPP overestimation in droughts. Finally, our method used to estimate the impacts of drought sensitivity change on C uptake could induce uncertainties, particularly under warming scenarios, because other factors such as plant acclimation and climate change were not considered (but are currently poorly constrained in the literature).

Ethics & Inclusion statement

This research involves collaborations of scientists in both America and Spain. All authors contribute to the study design, analysis, and results, and their names are listed in the title page. All data are publicly available from online resources. This is a continental scale study and no local partners or agencies are required. The authors declare no competing interest and agree on the roles and responsibilities related to this study. This research is not restricted or prohibited in the setting of the researchers. No animals, discrimination, health issues, or biological materials are relevant to this research.

DATA AVAILABILITY

The NTSG Landsat GPP data were obtained from the Google Earth Engine: https://developers.google.com/earth-engine/datasets/catalog. The GLASS GPP data were obtained from http://www.glass.umd.edu/Download.html. The EC-LUE GPP data were obtained from https://doi.org/10.6084/m9.figshare.8942336.v3. The NIRv GPP data were downloaded from https://doi.org/10.6084/m9.figshare.12981977.v2. The FLUXNET2015 GPP data set is available at https://fluxnet.org/data/fluxnet2015-dataset/. The historical climatic data (e.g. precipitation) and PDSI data were obtained from TerraClimate (https://www.climatologylab.org/terraclimate.html). The climatic data under +2 °C warming scenario were also obtained from TerraClimate (https://www.climatologylab.org/terraclimate.html). The MTBS maps of fire severity are available at https://www.mtbs.gov/direct-download. The land-cover maps were obtained from Earthdata (https://lpdaac.usgs.gov/products/mcd12q1v006/). The mean annual rates of mortality were from Anderegg et al. (2022)[11], and no new mortality data were produced. The US

boundary was from DATA.GOV (https://data.gov/). The data produced in this study are available from figshare[48] (doi:10.6084/m9.figshare.23730507): https://figshare.com/s/ace0046a5200b4451e82

CODE AVAILABILITY

All analysis was done in the open-source software R. The code is available from figshare[48] (doi:10.6084/m9.figshare.23730507): https://figshare.com/s/ace0046a5200b4451e82

Methods-only references

35. Robinson, N. P. *et al.* Terrestrial primary production for the conterminous United States derived from Landsat 30 m and MODIS 250 m. *Remote Sensing in Ecology and Conservation* **4**, 264–280 (2018).
36. Liang, S. *et al.* The Global Land Surface Satellite (GLASS) Product Suite. *Bulletin of the American Meteorological Society* **102**, E323–E337 (2021).
37. Zheng, Y. *et al.* Improved estimate of global gross primary production for reproducing its long-term variation, 1982–2017. *Earth System Science Data* **12**, 2725–2746 (2020).
38. Wang, S., Zhang, Y., Ju, W., Qiu, B. & Zhang, Z. Tracking the seasonal and inter-annual variations of global gross primary production during last four decades using satellite near-infrared reflectance data. *The Science of The Total Environment* **755**, 142569 (2020).
39. Wells, N., Goddard, S. & Hayes, M. J. A Self-Calibrating Palmer Drought Severity Index. *Journal of Climate* **17**, 2335–2351 (2004).
40. Abatzoglou, J. T., Dobrowski, S. Z., Parks, S. A. & Hegewisch, K. C. TerraClimate, a high-resolution global dataset of monthly climate and climatic water balance from 1958–2015. *Sci Data* **5**, 170191 (2018).
41. van der Schrier, G., Barichivich, J., Briffa, K. R. & Jones, P. D. A scPDSI-based global data set of dry and wet spells for 1901–2009. *Journal of Geophysical Research: Atmospheres* **118**, 4025–4048 (2013).
42. Aitken, A. C. On Least Squares and Linear Combination of Observations. *Proceedings of the Royal Society of Edinburgh* **55**, 42–48 (1936).
43. Breiman, L. Random Forests. *Machine Learning* **45**, 5–32 (2001).

44. Cao, S. *et al.* Spatiotemporally consistent global dataset of the GIMMS Leaf Area Index (GIMMS LAI4g) from 1982 to 2020. *Earth System Science Data Discussions* 1–31 (2023) doi:10.5194/essd-2023-68.

45. Cheng, W. *et al.* Global monthly gridded atmospheric carbon dioxide concentrations under the historical and future scenarios. *Sci Data* **9**, 83 (2022).

46. Qin, Y. *et al.* Agricultural risks from changing snowmelt. *Nat. Clim. Chang.* **10**, 459–465 (2020).

47. Stocker, B. D. *et al.* Drought impacts on terrestrial primary production underestimated by satellite monitoring. *Nat. Geosci.* **12**, 264–270 (2019).

48. Liu, M. *et al*. Forest sensitivity change in response to disturbances. figshare. Dataset. (2023) doi:10.6084/m9.figshare.23730507.

Climate-driven disturbances amplify forest drought sensitivity

Meng Liu[1,2], Anna T. Trugman[3], Josep Peñuelas[4,5], William R. L. Anderegg[1,2]

[1]School of Biological Sciences, University of Utah, Salt Lake City, UT, USA

[2]Wilkes Center on Climate Science and Policy, University of Utah, Salt Lake City, UT, USA

[3]Department of Geography, University of California Santa Barbara, Santa Barbara, CA, USA

[4]CREAF, Cerdanyola del Vallès, Barcelona, Catalonia, Spain

[5]CSIC, Global Ecology Unit CREAF-CSIC-UAB, Bellaterra, Barcelona, Catalonia, Spain

Corresponding author: Meng Liu (meng.liu@tamu.edu)

Abstract

Forests are a major terrestrial carbon sink, but the increasing frequency and intensity of climate-driven disturbances such as droughts, fires, and biotic agent outbreaks is threatening carbon uptake and sequestration. Determining how climate-driven disturbances may alter the capacity of forest carbon sinks in a changing climate is crucial. Here, we show that the sensitivity of gross primary productivity (GPP) to subsequent water stress increased significantly after initial drought and fire disturbances in the conterminous United States. Insect outbreak events, however, did not have significant impacts. Hot and dry environments generally exhibited increased sensitivity. Estimated ecosystem productivity and terrestrial carbon uptake decreased markedly with future warming scenarios due to the increased sensitivity to water stress. Our results highlight that intensifying disturbance regimes are likely to further impact forest sustainability and carbon sequestration, increasing potential risks to future terrestrial carbon sinks and climate change mitigation.

Main text

Terrestrial vegetation stores 450 Pg of carbon (C) and sequesters ~1.9 Pg C per year[1] (net C sink), which counterbalances approximately 20% of global C emissions from fossil fuel burning. As the primary driver of the terrestrial C sink, forests play a key role in regulating terrestrial ecosystems and the C cycle. Forests in the conterminous United States (CONUS) sequester 173 Tg C per year[2], and offset 9.7% of anthropogenic C emissions annually. Forest-based strategies to mitigate climate change, such as reforestation, improved forest management, and avoidance of forest loss, have been proposed as potentially impactful 'nature-based climate solutions' alongside dramatic reductions in fossil-fuel emissions[3,4]. However, disturbances that are sensitive to climate, such as droughts, fires, and insect outbreaks, decrease forest productivity, increase tree mortality, and decrease C storage, at least at short timescales[5–8]. At regional scales and over longer timescales, changes in disturbance regimes (e.g. more frequent and/or more severe disturbances) impair forest resistance (i.e. the capacity of the ecosystem to maintain its state and function[9]) and increase the risk of decreasing long-term C storage, which is crucial for mitigating climate change[10]. The frequency and intensity of prevalent disturbances, particularly droughts, fires, and those from biotic agents (e.g. insect outbreaks), are projected to increase in response to global warming[11–13] and will likely play a pivotal role in future forest C sink. Identifying the changes and dynamics of forest gross primary production (GPP) and how forests respond to environmental stressors after disturbances is paramount in systematically managing terrestrial ecosystems and effectively mitigating climate change.

Climate-driven disturbances have both direct and indirect effects on forest GPP. Direct effects often involve a concomitant decrease in GPP during disturbances. For example, the severe heat and drought event in 2003 led to a 30% decrease in ecosystem GPP in Europe[14], resulting in a strong anomalous net forest carbon source. However, these direct effects are typically short-lived for droughts, with forest GPP rebounding to pre-disturbance levels within a few months to a year[15]. Though, if trees die during fires and insect outbreaks, forest GPP recovery may take multiple years or longer. Indirect effects, on the other hand, refer to changes in the sensitivity of forest GPP to climate stressors after disturbances, which can persist for several years. The sensitivity of forest GPP to water stress, particularly water availability, is a critical measure of

response that indicates the "resistance" of forests to environmental variability and their capacity to sequester carbon. High sensitivity (low resistance) to water stress often signifies a high vulnerability to water deficits and climatic extremes, frequently preceding an increase in forest mortality[16]. The sensitivity of forest productivity, including GPP, tree-ring width, basal area growth, and greenness, to drought can be influenced by various factors, such as environmental conditions (soil, topography, and climate), stand composition (species and age), plant functional traits (wood density and hydraulic traits), and human management[9,17–24]. However, a comprehensive understanding of the indirect effects of disturbances on forest GPP is currently lacking. It remains unknown whether forest GPP becomes more or less sensitive to water stress after disturbances. Quantifying the long-term changes in the sensitivity of GPP to water stress in response to disturbances is crucial for enhancing our understanding and modeling the impacts of climate change on forest carbon cycling in the 21st century.

We aimed to investigate whether the sensitivity of ecosystem GPP to water stress changes after severe droughts, fires, and insect outbreaks. We examined the factors driving these changes and assessed their implications for carbon uptake. Leveraging long-term remotely sensed GPP data in CONUS, we performed regression analysis to understand the response of plant productivity to variations in water stress, as indicated by widely used drought indices like the Palmer Drought Severity Index (PDSI)[25] and the Standardized Precipitation–Evapotranspiration Index (SPEI)[26]. We calculated the sensitivity of forest GPP to water stress (referred to as "drought sensitivity") and compared it before and after disturbances. Machine learning models, specifically Random Forest regression, were employed to uncover the drivers and potential mechanisms underlying changes in drought sensitivity. We sought to answer the following research questions: 1) How does drought sensitivity change after severe disturbances across CONUS? 2) How do changes in drought sensitivity vary across different land-cover and ecosystem types? 3) What are the major factors influencing changes in drought sensitivity? 4) How might the observed changes in drought sensitivity affect vegetation carbon uptake under future warming scenarios?

Change in drought sensitivity at the continental scale

The drought sensitivity across CONUS changed significantly after severe droughts and fires. We illustrated how to calculate the change in GPP drought sensitivity with schematics (Fig. 1a and b). The sensitivity increased significantly after severe droughts and fires (Fig. 1c and d; Table S1 in Supplementary Information), where the means of the changes in sensitivity (Δk) were 3.80 ± 0.95 (mean ± standard error; p = 0.0001, GLS) and 3.83 ± 0.73 (p = 0, GLS) g C m^{-2}, respectively. Most pixels (59.12%) indicated increased sensitivity after severe droughts, but some pixels in eastern and northwestern CONUS manifested decreased sensitivity (Fig. 1c). Fewer pixels were available for analyzing the effects of fires, but the increase in sensitivity after fires was still significant (Fig. 1d), with 58.64% of the available pixels indicating increased sensitivity. The sensitivity, however, did not change significantly after insect outbreaks, −0.79 ± 1.23 (p = 0.52, GLS) g C m^{-2} (Fig. 1e). Forests in the northwest had decreased sensitivity after insect outbreaks, while Rocky Mountains had increased sensitivity. The results were similar when using SPEI to represent water stress (Extended Data Fig. 1a–c), where the sensitivity increased significantly across CONUS after severe droughts and fires, at 5.68 ± 2.06 (p = 0.0058, GLS) and 3.95 ± 1.73 (p = 0.023, GLS) g C m^{-2}, respectively, and decreased significantly after insect outbreaks, −6.22 ± 2.73 (p = 0.022, GLS) g C m^{-2}. We note as well that the patterns were robust when considering only pixels with significant GPP–PDSI relationships (Extended Data Fig. 2; Table S2). In summary, disturbances clearly altered GPP drought sensitivity, but the directions of the change in sensitivity diverged among disturbances and regions.

The sensitivity increased significantly (Δk = 6.21 ± 1.06 g C m^{-2}, p = 0, GLS; Table S3) in hot and dry regions (e.g. T > 10 °C and P < 1000 mm) (Fig. 1f) and did not change in cold and wet regions (e.g. T < 10 °C and P > 2000 mm) after severe droughts. The sensitivity increased significantly in hot and dry regions after fires (Δk = 5.33 ± 0.72 g C m^{-2}, p = 0, GLS), though there were almost no wet regions (only five pixels) (Fig. 1g), because fire was concentrated in dry regions. After insect outbreaks, the sensitivity did not change in hot and dry regions and decreased significantly in cold and wet regions (Δk = −28.49 ± 6.80 g C m^{-2}, p = 0.0002, GLS) (Fig. 1h). The intercept of the GPP–PDSI model decreased significantly after disturbances, where the means of the changes in the intercept (Δb) were all significantly lower than zero: −7.91 ± 3.51 (p

= 0.024, GLS), −7.73 ± 0.90 (p = 0, GLS), and −7.80 ± 1.94 (p = 0.0001, GLS) g C m^{-2} (Extended Data Fig. 3).

Change in drought sensitivity among land-cover types

The drought sensitivity of forests generally increased after severe disturbances, although with some notable differences among forest types. The sensitivity increased after severe droughts for evergreen needleleaf, evergreen broadleaf, and deciduous broadleaf forests (Extended Data Fig. 4, Fig. 2a, and Table S1), with the largest increase in deciduous broadleaf forests (5.47 ± 2.22 g C m^{-2}; p = 0.014, GLS). Evergreen and deciduous broadleaf forests were more sensitive to water stress after fires, and evergreen needleleaf forests were less sensitive, at −0.73 ± 0.45 g C m^{-2} (Fig. 2b). The change in the sensitivity was only significant in deciduous broadleaf forests, at 6.67 ± 3.08 (p = 0.031, GLS) g C m^{-2}. The drought sensitivity of forests did not change after insect outbreaks. The changes in the sensitivity of shrubland and grassland were large but not always significant. The changes in drought sensitivity were highly unlikely to be due to long-term trends, because undisturbed regions had different trends in sensitivity during 1982–2018 compared to disturbed regions with the same land-cover type (Extended Data Fig. 5). These results confirmed that the sensitivity of forests was affected by severe disturbances and that the sensitivity tended to increase after disturbances. The results were comparable when using SPEI (Extended Data Fig. 1d–f), where evergreen broadleaf and deciduous broadleaf forests exhibited significantly increased sensitivity, at 23.50 ± 8.14 (p = 0.0041, GLS) and 16.18 ± 7.04 (p = 0.022, GLS) g C m^{-2}, after severe droughts.

The intercept of the GPP–PDSI model decreased in forests (Fig. 2 and Table S1). The decreases were due to lower biomass and foliar area caused by disturbances, leading to decreased forest productivity. The directions of the changes in the intercept were not consistent for grassland and shrubland. It is very intriguing that the intercept of shrubland increased after all three disturbances, which might indicate that the direct effects (GPP decrease) of disturbances on shrubland can recover quickly. However, the intercept change is not strictly related to the absolute GPP change since we used detrended GPP. From the perspective of vegetation structure, shrubs have smaller leaf area, frequent resprouting behaviors, and shorter canopy heights than forests, which might benefit the recovery of shrubland productivity after disturbances.

Factors influencing the change in drought sensitivity

Several climatic factors play a crucial role in driving the change in drought sensitivity. These factors include the trend of soil moisture (Trend.SM), mean annual temperature (MAT), the interaction between temperature and reversed precipitation (Interaction.TP), and downward surface shortwave radiation (Srad). For drought, the Random Forest model explained 67% of the variation (R^2 = 0.67; Extended Data Fig. 6a) in the change in sensitivity, with the trend of soil moisture emerging as the most important driver (Fig. 3a). Mean annual temperature and the interaction between temperature and reversed precipitation ranked as the second and third most important drivers, respectively. The change in sensitivity increased with decreasing trends of soil moisture (Fig. 3b), indicating that lower soil moisture levels contributed to higher post-disturbance sensitivity. Similarly, the change in sensitivity increased with mean annual temperature (Fig. 3c), suggesting that regions experiencing higher temperatures were more likely to exhibit increased sensitivity after disturbances. The interaction between temperature and reversed precipitation (Fig. 3d) had similar effects to mean annual temperature, with higher values (indicating hot and dry regions) associated with increased drought sensitivity.

For fires and insect outbreaks, the Random Forest models explained 37% and 28% of the variations in sensitivity change, respectively (Extended Data Fig. 6b and c). Mean annual temperature emerged as the most important driver for fires (Fig. 3e), where regions with higher temperatures were associated with increases in sensitivity after the disturbance (Fig. 3f), particularly when mean annual temperature exceeded approximately 15°C. Additionally, increasing downward surface shortwave radiation (particularly when the trend of Srad is greater than zero) and a high PDSI were linked to an increase in sensitivity after fires. In the case of insect outbreaks, mean annual downward surface shortwave radiation emerged as the most important driver (Fig. 3i), with regions experiencing high radiation (e.g. > 180 W m^{-2}) demonstrating increased sensitivity, while regions with low radiation exhibited decreased sensitivity after the disturbance (Fig. 3j). This result aligns with the distribution of sensitivity change after insect outbreaks (Fig. 1e), where northwest regions generally displayed decreased sensitivity and low levels of shortwave radiation. Increasing trends in CO_2 and shortwave radiation also contributed to the increase in sensitivity after insect outbreaks (Fig. 3k and l).

Impacts on C uptake

The change in drought sensitivity of GPP has notable implications for C uptake and loss. We quantified C uptake responses to water stress and assessed the recovery time by utilizing pixels with a post-disturbance period of at least 16 years (see Methods). It took approximately five years for the sensitivity to return to the pre-disturbance level after severe droughts and around six years after fires (Extended Data Fig. 7b and c). Due to the relatively short post-disturbance time (nine years: 2010–2018), the recovery time for insect outbreaks was not calculated. We further estimated the potential change in C uptake resulting from the sensitivity change. As a first-order exploration, the change in C uptake was calculated as the difference in GPP when considering the changes in sensitivity and intercept (equation (2)). For drought, the mean annual change in C uptake over the five-year period following the disturbance was −9.94 ± 2.99 Tg C (Fig. 4a) across CONUS, indicating a reduction in C absorption. For fires, the mean annual change in C uptake over the six-year period after the disturbance was −1.50 ± 0.03 Tg C (Fig. 4c). To assess the effects of future warming, PDSI under +2 °C warming scenario was used to estimate the change in C uptake in response to the sensitivity change. For drought, the change in C uptake under the +2 °C warming scenario was estimated to be −11.21 ± 2.42 Tg C (Fig. 4b), indicating even lower C absorption than historical conditions. For fires, the change in C uptake was estimated to be −1.63 ± 0.04 Tg C under the warming scenario (Fig. 4d).

Implications for climate change mitigation

Severe disturbances, such as severe droughts, fires, and insect outbreaks, have significant impacts on forest ecosystems. They all have the potential to alter forest composition, leading to a shift towards early succession species[27], and can cause physiological damage to surviving trees. Both effects influence the sensitivity of post-disturbance forest productivity to water availability. This study specifically examines the indirect effects of severe disturbances and highlights the changes in GPP drought sensitivity following these extreme events. We have observed that severe disturbances, such as severe droughts and fires, tend to increase the sensitivity of forest productivity to water availability. This is particularly notable in deciduous broadleaf forests, possibly due to drought legacy effects[28] and disturbance-induced damage, such as embolism and overheating. These factors make trees more susceptible to subsequent water stress. Additionally,

for deciduous trees, physiological traits such as shallow roots[29] and thin bark likely contribute to increased susceptibility to fire and drought damage. In contrast, for evergreen needleleaf forests, the sensitivity did not change and even decreased after fires and insect outbreaks. This phenomenon may be attributed to decreases in stand density following disturbances. Generally, stand density has increased in many evergreen needleleaf forests in the western United States due to historical fire suppression activities[30]. Disturbances can relax overstocked conditions and reduce competition[31] for water. This result suggests that thinning holds the potential to alleviate water stress in certain conifer forests. Additionally, gymnosperm-dominated forests, mainly needleleaf forests in the western United States, have shown notable shifts characterized by decreases in P50 (water potential at which 50% of conductivity is lost) and increases in HSM (hydraulic safety margin, the difference between P50 and the minimum water potential experienced)[32] in response to climate-driven mortality, making these forests more drought-tolerant.

Non-forested ecosystems, such as shrublands and grasslands, also exhibit heightened drought sensitivity following disturbances, especially after severe droughts and fires. This increased sensitivity may be attributed to their proximity to absolute biogeographic and climate thresholds. Shrubs and grasses predominantly thrive in arid regions characterized by high solar radiation and temperature coupled with low water availability. Moreover, dry regions, particularly shrublands and grasslands, reveal stronger correlations between GPP and PDSI (Extended Data Fig. 2b). Climate emerges as a crucial factor influencing sensitivity changes, with hot and dry regions experiencing increased sensitivity and cold and wet regions showing decreased sensitivity (Fig. 1). Previous research[28] also indicates that plants in arid regions exhibit stronger drought legacy effects compared to those in wet regions.

Droughts, fires, and insect outbreaks have varied impacts on ecosystems. In general, understory species such as grasses and herbs are sensitive to water availability[33] and usually senesce rapidly due to water deficits. During droughts, both the understory and overstory vegetation will be constrained. The absolute GPP values of understory grasses might recover in the next year; however, the GPP sensitivity to water (i.e. indirect effects) of the whole ecosystem, including both the understory and overstory vegetation, may not recover as quickly. The

sensitivity of grasslands increased significantly (p = 0, GLS) after droughts (Fig. 2a), indicating that the GPP sensitivity of grasses may not necessarily recover at the same pace as the absolute GPP. For overstory trees, drought legacy effects can last for years[28]. A similar situation goes for fires, where both the understory grasses and overstory trees might be burned during fires. The absolute GPP of understory grasses can recover quickly; however, the GPP sensitivity might not (Fig. 2b). For overstory trees, fire damage, such as heat stress (e.g. heat emboli) and biomass consumption, can cause a long-lasting sensitivity change. For insect outbreaks, understory grasses are not the target of widespread insects like bark beetles[7], and thus the impacts of insects on understory vegetation will be small. The unchanged (or even decreased) sensitivity after insect outbreaks could be due to the decreases in stand density and shifts in composition.

Across CONUS, the increased sensitivity of GPP to water stress leads to substantial decreases in C uptake after severe droughts and fires. These decreases are logical as photosynthesis and C uptake tend to decline more when sensitivity increases at the same level of water stress, and climate change is likely to bring more frequent and severe droughts in many regions. Our estimates suggest that the decrease in C uptake can persist for approximately 5~6 years after the disturbances. This reduction in C uptake hampers the capacity of terrestrial ecosystems to sequester anthropogenic C emissions. Furthermore, our findings highlight the accelerated decline in C uptake under warming scenarios. Less carbon would be absorbed in response to increased sensitivity under warming scenarios compared to historical conditions. Many regions in CONUS are projected to experience hotter and drier conditions under future warming scenarios[13], leading to increased water stress on plant growth. As a result, ecosystems' ability to absorb carbon would decline, exacerbated by increased water stress and vegetation sensitivity. Regions such as western North America face high risks of carbon loss and species loss due to climate change, as indicated by global assessments[34].

Climate change is expected to increase the frequency and severity of disturbances in many regions. From the perspective of climate policy and management, relying on planting more trees to counterbalance C emissions from fossil fuel burning can be challenging, particularly when ecosystem productivity is threatened by disturbances that are climate dependent. Our results highlight pervasive changes in the drought sensitivity of GPP in forests after disturbances and

imply meaningful impacts on C uptake. Increased sensitivity increases the vulnerability of ecosystems to drought and could lead to substantial decreases in ecosystem C uptake under future warming scenarios. These long-term dynamics are important for evaluating the capacity of terrestrial ecosystems as C sinks for C management, nature-based climate solutions, and net-zero pledges.

Acknowledgements

The study was supported by the Wilkes Center at the University of Utah, and thanks to the Anderegg lab. J.P. was supported by the TED2021-132627B-I00 grant, funded by MCIN and the European Union NextGeneration EU/PRTR, and the CIVP20A6621 grant funded by the Fundación Ramón Areces. A.T.T. acknowledges funding from National Science Foundation Grants 2003205, 2017949 and 2216855, the University of California Laboratory Fees Research Program Award No. LFR-20-652467, and the Gordon and Betty Moore Foundation Grant GBMF11974. W.R.L.A. acknowledges support from the David and Lucille Packard Foundation and US National Science Foundation grants 1802880, 2003017 and 2044937.

Author Contributions Statement

M.L. and W.R.L.A. conceptualized and designed the study with input from all co-authors. M.L. performed the analysis. M.L. wrote the initial draft and A.T.T., J.P. and W.R.L.A. discussed the design, analyses and results and provided extensive and valuable comments and revisions.

Competing Interests Statement

The authors declare no competing interests.

Figure Legends/Captions

Fig. 1 The sensitivity of vegetation to water stress in CONUS changed significantly after severe disturbances. (**a**–**b**) Schematics of (**a**) GPP anomalies (detrended) and PDSI, and (**b**) change in sensitivity due to disturbances. (**c**–**e**) The change in sensitivity after severe (**c**) droughts, (**d**) fires, and (**e**) insect outbreaks. Asterisks indicate significance at the 0.05 level (two-sided) based on the generalized least squares (GLS) model. Multiple comparisons are not applicable. The distribution maps (4 km) for fires and insect outbreaks were aggregated to 20 km for visual

display. (**f**–**h**) The change in sensitivity in climate space (mean annual temperature (MAT) vs mean annual precipitation (MAP); 1 °C ×100 mm grid).

Fig. 2 The drought sensitivity of forests increased after severe disturbances. The mean changes in sensitivity (Δ*k*) and intercept (Δ*b*) for different land covers in CONUS after severe (**a**) droughts (left to right, *N*=2401, 414, 4691, 1127, 7719), (**b**) fires (*N*=1944, 178, 258, 601, 6068), and (**c**) insect outbreaks (*N*=7320, 111, 548, 157, 3904). The error bars are standard errors, and the asterisks indicate that the mean is significant at the 0.05 level (two-sided) based on the GLS model. Multiple comparisons are not applicable. ENF, evergreen needleleaf forest; EBF, evergreen broadleaf forest; DBF, deciduous broadleaf forest.

Fig. 3 Drivers of the change in GPP drought sensitivity. (**a**–**d**) Drivers of the change in the sensitivity of GPP to water stress after severe droughts: (**a**) importance of drivers and (**b**–**d**) Random Forest partial dependence of the change in sensitivity on the three most important drivers. (**e**–**h**) Drivers of the change in the sensitivity of GPP to water stress after severe fires. (**i**–**j**) Drivers of the change in the sensitivity of GPP to water stress after severe insect outbreaks. The solid black line is the average, and the shading shows the range (i.e. from minimum to maximum) of the partial dependence from 100 runs of Random Forest models.

Fig. 4 Carbon (C) uptake decreases in warming scenarios. (**a**–**b**) The average change in C uptake (ΔC) due to the change in sensitivity after severe droughts under (**a**) historical time and (**b**) +2 °C warming scenario. (**c**–**d**) The average ΔC due to the change in sensitivity after severe fires. 'Annual' indicates mean annual total ΔC across CONUS, and the asterisk indicates the mean is significant at the 0.05 level (two-sided, both GLS models and t test). Multiple comparisons are not applicable. Panels **c**–**d** are aggregated to 20 km for visual display.

References

1. Friedlingstein, P. *et al.* Global Carbon Budget 2022. *Earth System Science Data* **14**, 4811–4900 (2022).
2. Wear, D. N. & Coulston, J. W. From sink to source: Regional variation in U.S. forest carbon futures. *Sci Rep* **5**, 16518 (2015).
3. Griscom, B. W. *et al.* Natural climate solutions. *PNAS* **114**, 11645–11650 (2017).

4. Fargione, J. E. *et al.* Natural climate solutions for the United States. *Science Advances* **4**, eaat1869 (2018).
5. Seidl, R. *et al.* Forest disturbances under climate change. *Nature Clim Change* **7**, 395–402 (2017).
6. McDowell, N. G. & Allen, C. D. Darcy's law predicts widespread forest mortality under climate warming. *Nature Clim Change* **5**, 669–672 (2015).
7. Williams, C. A., Gu, H., MacLean, R., Masek, J. G. & Collatz, G. J. Disturbance and the carbon balance of US forests: A quantitative review of impacts from harvests, fires, insects, and droughts. *Global and Planetary Change* **143**, 66–80 (2016).
8. Hemes, K. S., Norlen, C. A., Wang, J. A., Goulden, M. L. & Field, C. B. The magnitude and pace of photosynthetic recovery after wildfire in California ecosystems. *Proceedings of the National Academy of Sciences* **120**, e2201954120 (2023).
9. Anderegg, W. R. L., Trugman, A. T., Badgley, G., Konings, A. G. & Shaw, J. Divergent forest sensitivity to repeated extreme droughts. *Nat. Clim. Chang.* **10**, 1091–1095 (2020).
10. Anderegg, W. R. L. *et al.* Climate-driven risks to the climate mitigation potential of forests. *Science* **368**, eaaz7005 (2020).
11. Anderegg, W. R. L. *et al.* Future climate risks from stress, insects and fire across US forests. *Ecology Letters* **25**, 1510–1520 (2022).
12. Dai, A. Drought under global warming: a review. *WIREs Climate Change* **2**, 45–65 (2011).
13. Cook, B. I., Ault, T. R. & Smerdon, J. E. Unprecedented 21st century drought risk in the American Southwest and Central Plains. *Science Advances* **1**, e1400082 (2015).
14. Ciais, P. *et al.* Europe-wide reduction in primary productivity caused by the heat and drought in 2003. *Nature* **437**, 529–533 (2005).
15. Schwalm, C. R. *et al.* Global patterns of drought recovery. *Nature* **548**, 202–205 (2017).
16. Keen, R. M. *et al.* Changes in tree drought sensitivity provided early warning signals to the California drought and forest mortality event. *Global Change Biology* **28**, 1119–1132 (2022).
17. Fu, Z. *et al.* Sensitivity of gross primary productivity to climatic drivers during the summer drought of 2018 in Europe. *Philosophical Transactions of the Royal Society B: Biological Sciences* **375**, 20190747 (2020).

18. Phillips, R. P. *et al.* A belowground perspective on the drought sensitivity of forests: Towards improved understanding and simulation. *Forest Ecology and Management* **380**, 309–320 (2016).
19. McDowell, N. *et al.* Mechanisms of plant survival and mortality during drought: why do some plants survive while others succumb to drought? *New Phytologist* **178**, 719–739 (2008).
20. Cartwright, J. M., Littlefield, C. E., Michalak, J. L., Lawler, J. J. & Dobrowski, S. Z. Topographic, soil, and climate drivers of drought sensitivity in forests and shrublands of the Pacific Northwest, USA. *Sci Rep* **10**, 18486 (2020).
21. Rosner, S. *et al.* Wood density as a screening trait for drought sensitivity in Norway spruce. *Can. J. For. Res.* **44**, 154–161 (2014).
22. Mausolf, K. *et al.* Higher drought sensitivity of radial growth of European beech in managed than in unmanaged forests. *Science of The Total Environment* **642**, 1201–1208 (2018).
23. Lebourgeois, F., Gomez, N., Pinto, P. & Mérian, P. Mixed stands reduce Abies alba tree-ring sensitivity to summer drought in the Vosges mountains, western Europe. *Forest Ecology and Management* **303**, 61–71 (2013).
24. Linares, J. C., Taïqui, L., Sangüesa-Barreda, G., Seco, J. I. & Camarero, J. J. Age-related drought sensitivity of Atlas cedar (Cedrus atlantica) in the Moroccan Middle Atlas forests. *Dendrochronologia* **31**, 88–96 (2013).
25. Palmer, W. C. Meteorological drought. *U.s.department of Commerce Weather Bureau* (1965).
26. Beguería, S., Vicente-Serrano, S. M., Reig, F. & Latorre, B. Standardized precipitation evapotranspiration index (SPEI) revisited: parameter fitting, evapotranspiration models, tools, datasets and drought monitoring. *International Journal of Climatology* **34**, 3001–3023 (2014).
27. Trugman, A. T., Medvigy, D., Anderegg, W. R. L. & Pacala, S. W. Differential declines in Alaskan boreal forest vitality related to climate and competition. *Global Change Biology* **24**, 1097–1107 (2018).
28. Anderegg, W. R. L. *et al.* Pervasive drought legacies in forest ecosystems and their implications for carbon cycle models. *Science* **349**, 528–532 (2015).

29. Tumber-Dávila, S. J., Schenk, H. J., Du, E. & Jackson, R. B. Plant sizes and shapes above and belowground and their interactions with climate. *New Phytologist* **235**, 1032–1056 (2022).
30. Voelker, S. L. *et al.* Fire deficits have increased drought sensitivity in dry conifer forests: Fire frequency and tree-ring carbon isotope evidence from Central Oregon. *Global Change Biology* **25**, 1247–1262 (2019).
31. Sheil, D. Disturbance and distributions: avoiding exclusion in a warming world. *Ecology and Society* **21**, (2016).
32. Trugman, A. T., Anderegg, L. D. L., Shaw, J. D. & Anderegg, W. R. L. Trait velocities reveal that mortality has driven widespread coordinated shifts in forest hydraulic trait composition. *Proceedings of the National Academy of Sciences* **117**, 8532–8538 (2020).
33. Adhikari, A. *et al.* Management and climate variability effects on understory productivity of forest and savanna ecosystems in Oklahoma, USA. *Ecosphere* **12**, e03576 (2021).
34. Anderegg, W. R. L. *et al.* A climate risk analysis of Earth's forests in the 21st century. *Science* **377**, 1099–1103 (2022).

Methods

Data

We used gross primary production (GPP) to indicate the photosynthetic capacity and productivity of forests. Four state-of-the-art long-term GPP datasets covering CONUS were used: the Numerical Terradynamic Simulation Group (NTSG) Landsat GPP data set[35], the Global LAnd Surface Satellite (GLASS) GPP data set[36], the revised Eddy Covariance-Light Use Efficiency (EC-LUE) model derived GPP data set[37], and the near-infrared reflectance of vegetation (NIRv) based GPP data set[38]. The NTSG GPP data set (1986–2021) provided 16-day 30-m GPP data based on Landsat data and climatic variables across CONUS. (See Supplementary Information for details on these GPP products.) The four sets of GPP data were resampled to 4 km and aggregated to the annual level. Anomalies were calculated and detrended for each pixel for each GPP product. The four detrended anomalies were averaged for each pixel for all subsequent analysis to avoid inconsistencies and biases among the GPP products. The following analysis was based on the average anomalies of the four GPP products from 1982 to 2018.

We utilized two widely recognized drought indices, namely the Palmer Drought Severity Index (PDSI)[25,39] and the Standardized Precipitation–Evapotranspiration Index (SPEI)[26], to quantify water stress and calculate changes in GPP drought sensitivity. The PDSI is a standardized metric derived from a two-layer soil water balance model, where negative values indicate dry conditions and positive values indicate wet conditions. We obtained monthly historical PDSI data at a 4-km resolution covering the period between 1982 and 2018 from TerraClimate[40], which provides climatic variables such as temperature (T), precipitation (P), soil moisture (SM), potential evapotranspiration (PET), and downward surface shortwave radiation (Srad). The PDSI data from TerraClimate were based on the Penman–Monteith equation-based PET. Monthly PDSI values were averaged to generate annual PDSI data. Severe drought disturbances were defined as annual PDSI values below -3[25,41]. Other thresholds such as -2 and -4 were also tested, and the results were comparable when using -3 and -4. -2 usually indicates moderate droughts, which have limited effects on ecosystems. The SPEI is a multi-scalar drought index that captures atmospheric water deficits by considering the difference between precipitation and PET. In our analysis, we used monthly precipitation and PET data from TerraClimate at a 4-km resolution to

calculate the monthly 4-km SPEI12 (scale = 12-month) between 1982 and 2018 using the "SPEI" package in R. SPEI12 was selected as we used annual data in this study. Monthly SPEI12 values were averaged to the annual level, and severe droughts were defined as SPEI12 values below -1.2[9]. Other thresholds such as -1 and -1.5 were also tried, and the results were comparable when using -1.2 and -1.5. -1 is usually related to moderate droughts, which have limited impacts on ecosystems.

Maps of annual fire severity were obtained from the Monitoring Trends in Burn Severity (MTBS) database, which has provided fire maps for the United States since 1984. The 30-m resolution maps of annual fire severity between 1984 and 2018 were downloaded and aggregated to 4 km. Low-severity pixels were discarded because low-severity fires generally have very small impacts on forests. The proportion of burned 30-m pixels (moderate- and high-severity pixels) within each 4-km grid was calculated when aggregating the 30-m pixels to 4-km data. A 4-km grid was treated as burned when the proportion was > 10%. Plots from the Forest Inventory and Analysis (FIA) program were used to identify damage caused by insect outbreaks. Agent Codes (AGENTCD) of 10–19 for the FIA plots indicates that insects caused mortality. The rates of mortality of basal area due to insects were used to indicate insect damage. The mean annual rate of mortality for each plot during 2000–2009 was taken from Anderegg et al. (2022)[11]. We aggregated the plots to 4 km and calculated the average rate for each pixel. An average rate > 0.3% was used to define insect outbreaks. The species of biotic agents (particularly insects here) were not provided by the FIA data.

Land-cover maps at a resolution of 500 m from the Terra and Aqua combined MODIS Land Cover Type (MCD12Q1) Version 6 from 2001 to 2020 were used to identify different vegetation types. Land-cover type 5 was used, where croplands and non-vegetation (water, urban, and barren) classes were removed. Pixels with changes in land cover in 2001–2020 were also removed. We aggregated the 500-m land-cover maps to 4 km to match the GPP data. The land-cover map for 2001 is shown in Extended Data Fig. 4.

Analysis of sensitivity

The slope of a linear regression (GPP anomaly vs PDSI) was used to represent the sensitivity of photosynthesis to water availability because most pixels (~70%) in CONUS presented a linear relationship between GPP anomaly and PDSI (Extended Data Fig. 2). Those pixels presenting non-linear relationships were dominated by grasslands. Thus, while a minority of areas do not have linear GPP–PDSI relationships, our results are robust to including only significant linear relationship pixels (Extended Data Fig. 2d–f and Table S2) and a linear model represents the most parsimonious, comparable, and understandable model of drought sensitivity and thus we used it for all analyses. We compared simple linear regression and multiple linear regression when deriving the sensitivity of GPP to water stress, where the sensitivity from the two models was significantly correlated (Extended Data Fig. 8). For droughts, the slope of the linear regression between pre-drought GPP anomalies and PDSI was calculated to indicate pre-drought sensitivity (k_0). Similarly, post-drought sensitivity (k_1) was calculated using post-drought GPP anomalies and PDSI. The difference between the post-drought and pre-drought slopes was treated as the change in sensitivity (Δk).

$$\begin{cases} \text{GPP anomaly}_{\text{pre}} = k_0 \times \text{PDSI}_{\text{pre}} + b_0 \\ \text{GPP anomaly}_{\text{post}} = k_1 \times \text{PDSI}_{\text{post}} + b_1 \\ \Delta k = k_1 - k_0,\ \Delta b = b_1 - b_0 \end{cases} \quad (1)$$

where b_0 and b_1 are intercepts. The change in sensitivity derived with SPEI12 was calculated in the same way shown in equation (1), where SPEI12 was used to indicate water stress.

We required at least eight years of data for regression when calculating the slopes. Based on the histogram of drought return intervals in Extended Data Fig. 9a, eight was the first break point for drought return intervals, and the disturbance return intervals of most pixels are higher than eight years. We also tried six (the trough) and ten (the second break point) years as the minimum for regression, and the corresponding changes in sensitivity were shown in Extended Data Fig. 9c and d, respectively, which were comparable to the change in sensitivity (Δk) in Fig. 2a. Eight years strikes a reasonable balance between sample size and stability. A lower threshold, such as six years, could make the results of linear regression unstable, whereas a higher threshold would decrease the sample size. For fire (Extended Data Fig. 9b), the return intervals of most

pixels were greater than ten years, indicating that any values lower than or equal to ten were acceptable. Therefore, using eight as the minimum number of years for regression was reasonable. The length of pre-disturbance and post-disturbance data could vary, and eight years was the minimum we used for regression analysis. The first drought was checked for each pixel. The change in sensitivity was calculated when we had at least eight data points for a regression analysis before and after the first drought. Otherwise, the second drought would be checked. This pixel was discarded if all droughts were not qualified for calculating the change in sensitivity. Continuous droughts were treated as one drought when calculating the change in sensitivity. When there were two or more drought events suitable for calculating Δk, the first one would be used. The same procedure was applied to fires, producing the change in sensitivity after a fire. For insect outbreaks, we calculated the slope between GPP anomalies and PDSI before 2000 to represent pre-outbreak sensitivity, and the slope after 2009 was treated as the post-outbreak sensitivity. We resorted to this approximation due to the limited availability of standardized FIA plots, which were only accessible from 2000 onwards and repeated every five or ten years. While the strategy employed to calculate the change in sensitivity for insect outbreaks may not be ideal, it was a reasonable approach given the data constraints. To validate our findings, we conducted a sensitivity analysis by separately analyzing the four GPP anomalies and the PDSI data. The results (Extended Data Fig. 10) were comparable to those obtained using the average anomalies of the four GPP products. The sensitivity change of each land-cover type based on a single GPP product was presented in Table S4.

To account for spatial autocorrelations in the changes in sensitivity (Δk) and intercept (Δb), we employed the generalized least squares (GLS) model[42] and examined their significance. We utilized the gls function from the "nlme" package in R. The exponential correlation structure, corExp, was selected to assess the significance of the mean Δk and mean Δb by fitting GLS models with the formulas "$\Delta k \sim 1$" and "$\Delta b \sim 1$" (regression with only the constant term), respectively. We experimented with five correlation structures: exponential, sphere, gaussian, ratio, and linear. The exponential correlation structure was always ranked in the top two correlation structures for minimizing AIC. So, to save time for computation (GLS models are extremely time-consuming when dealing with large samples), we decided to use the exponential correlation structure

494 throughout the manuscript. Due to computational intensity, we aggregated the Δ*k* and Δ*b* maps
495 for drought disturbances using a factor of three (4 km to 12 km) during the calculation. If the *p*-
496 value (two-sided) was below 0.05 based on the GLS, the constant term (i.e. mean Δ*k* or mean Δ*b*)
497 was considered significant.

498 **Random Forest model**

499 We employed Random Forest regression[43], a widely-used machine learning model, to
500 capture the change in sensitivity (equation (1)) and identify the primary drivers responsible for
501 this change. Random Forest regression, which utilizes an ensemble of decision trees, is well-
502 suited for analyzing high-dimensional data, such as large sample sizes with numerous predictors
503 and complex structure. To train the Random Forest model, we utilized the "randomForest"
504 package in R. The response variable was the change in sensitivity (Δ*k*), and the predictors included
505 various variables, namely temperature (T), precipitation (P), soil moisture (SM), downward
506 surface shortwave radiation (Srad), PDSI, leaf area index (LAI)[44], and CO_2 concentration[45]. For
507 each pixel, we calculated the long-term mean (e.g. mean annual temperature) and trend (e.g. the
508 trend of temperature, which is the slope of linear regression between T and year) of these
509 variables using data from 1982 to 2018. Additionally, we incorporated the interaction between T
510 and P (Interaction.TP) as a predictor, which represented the mean quantiles of T and reversed P.
511 First, we calculated the quantiles (0–1) of T, and high T had high quantiles. Second, we reversed
512 P by multiplying −1 (i.e. −1×P) and calculated the quantiles of the reversed P. Finally, we averaged
513 the quantiles of T and reversed P. The average quantiles can represent the interaction between
514 T and P, where high quantiles imply hot and dry conditions. GPP anomalies in the disturbed years
515 and land-cover types were also included as extra predictors. Prior to training the models, highly
516 correlated predictors were removed. For instance, when mean annual precipitation and mean
517 annual soil moisture exhibited a high correlation ($|r| > 0.7$), the predictor with a lower correlation
518 with Δ*k* was eliminated. In the Random Forest models, we used 500 decision trees, and the
519 number of splits was determined as the square root of the number of selected predictors ($\lfloor\sqrt{n}\rfloor$).
520 The LAI data were obtained from the half-month 8-km Global Inventory Modeling and Mapping
521 Studies (GIMMS) LAI4g product (1982–2020)[44], which were resampled (bilinear) to 4 km and
522 averaged to the annual level. Similarly, the global monthly 1° historical CO_2 concentration data[45]

from 1982 to 2013 were resampled (bilinear) to 4 km and averaged to the annual level. Separate Random Forest models were developed for each of the three disturbances, as the drivers varied among them. The resulting partial dependence plots generated by the Random Forest models illustrated the relationships between Δk and the predictors. Predictor importance was assessed based on the decrease in node purity, where the importance of a predictor was calculated as the decrease in node purity attributed to that predictor divided by the sum of the decrease in node purity for all predictors, multiplied by 100%. We ran the Random Forest models 100 times and averaged the responses (i.e. importance and partial dependence) of the 100 models (Fig. 3).

Recovery time and C uptake change

Recovery time was determined as the duration required for the sensitivity to return to its pre-disturbance level. Since the sensitivity could increase following disturbances, ecosystems may take years to recover their original states. To derive the recovery time, we selected pixels with a post-disturbance time of at least 16 years, ensuring a minimum of two independent eight-year periods to calculate sensitivity. A moving window strategy, utilizing eight-year intervals, was employed to compute post-disturbance sensitivity for each selected pixel. Within each moving window (1–8 years, 2–9 years, 3–10 years, etc.), the sensitivity was determined as the slope of linear regression between GPP anomaly and PDSI. We considered ecosystems to have recovered when the post-disturbance sensitivity was equal to or lower than the pre-disturbance sensitivity (k_0). The recovery time was defined as the first year of the moving window when the post-disturbance sensitivity was $\leq k_0$. The calculation of recovery time is illustrated in the schematic provided in Extended Data Fig. 7a, which exemplifies a recovery time of 5 years. If the sensitivity decreased after disturbances, the recovery time would be identified when the post-disturbance sensitivity was $\geq k_0$. The average recovery times for severe droughts and fires were 4.8 and 5.6 years, respectively. However, the recovery time for insect outbreaks could not be determined due to the limited post-disturbance period of nine years (2010–2018).

The change in carbon (C) uptake was estimated based on the change in GPP. The equation below represents the change in GPP (ΔGPP) in response to the change in sensitivity after disturbances:

$$\Delta GPP = \Delta k \times PDSI + \Delta b \quad (2)$$

where ΔGPP indicates the change in productivity, and Δ*k* and Δ*b* represent the changes in sensitivity and intercept, respectively (as shown in Fig. 1 and Extended Data Fig. 3). Historical PDSI data after disturbances were used to derive the change in C uptake (ΔC = ΔGPP). For severe droughts, the closest integer to 4.8 (i.e. 5 years) was employed, while for severe fires, the closest integer to 5.6 (i.e. 6 years) was used. Each pixel was associated with five PDSI values after severe droughts and six PDSI values after severe fires, which were inputted into equation (2) to calculate the corresponding ΔC. For instance, if a severe drought occurred in the tenth year, PDSI values in the eleventh, twelfth, thirteenth, fourteenth, and fifteenth years would be used in equation (2), producing five ΔGPP values. The mean annual ΔC per pixel after severe droughts and fires is presented in Fig. 4a and d, respectively, indicating a reduction in C assimilation through photosynthesis due to disturbances.

In warming scenarios, we utilized 4-km monthly precipitation and PET data under +2 °C warming obtained from Qin et al. (2020)[46] to generate PDSI values under the +2 °C scenario with the "scPDSI" package in R. The precipitation and PET data under the +2 °C scenario corresponded to the nominal years of 1985–2015. Monthly PDSI values under the warming scenario were calculated and averaged to the annual level. The change in C uptake was estimated using the annual PDSI values under the warming scenario following the same approach outlined in equation (2), with Δ*k* and Δ*b* obtained from Fig. 1 and Extended Data Fig. 3, respectively. The mean annual ΔC under the warming scenario is depicted in Fig. 4.

Caveats

The GPP products used in this study are based on different inputs and models, leading to inherent differences in results when comparing across different GPP datasets. To increase the robustness of our analysis, we used a detrended, ensemble mean approach when deriving GPP for our study. Though we believe that taking an ensemble mean strengthens the analysis above any based on a single product along, caution should be exercised in interpretation remote sensing based GPP data, which tend to overestimate vegetation productivity in droughts (particularly severe droughts[47]). To overcome the drought limitation in this study, we used pre-drought and

post-drought GPP data to conduct regression analysis, rather than data during drought. This approach avoids the potential limitations of GPP overestimation in droughts. Finally, our method used to estimate the impacts of drought sensitivity change on C uptake could induce uncertainties, particularly under warming scenarios, because other factors such as plant acclimation and climate change were not considered (but are currently poorly constrained in the literature).

Ethics & Inclusion statement

This research involves collaborations of scientists in both America and Spain. All authors contribute to the study design, analysis, and results, and their names are listed in the title page. All data are publicly available from online resources. This is a continental scale study and no local partners or agencies are required. The authors declare no competing interest and agree on the roles and responsibilities related to this study. This research is not restricted or prohibited in the setting of the researchers. No animals, discrimination, health issues, or biological materials are relevant to this research.

DATA AVAILABILITY

The NTSG Landsat GPP data were obtained from the Google Earth Engine: https://developers.google.com/earth-engine/datasets/catalog. The GLASS GPP data were obtained from http://www.glass.umd.edu/Download.html. The EC-LUE GPP data were obtained from https://doi.org/10.6084/m9.figshare.8942336.v3. The NIRv GPP data were downloaded from https://doi.org/10.6084/m9.figshare.12981977.v2. The FLUXNET2015 GPP data set is available at https://fluxnet.org/data/fluxnet2015-dataset/. The historical climatic data (e.g. precipitation) and PDSI data were obtained from TerraClimate (https://www.climatologylab.org/terraclimate.html). The climatic data under +2 °C warming scenario were also obtained from TerraClimate (https://www.climatologylab.org/terraclimate.html). The MTBS maps of fire severity are available at https://www.mtbs.gov/direct-download. The land-cover maps were obtained from Earthdata (https://lpdaac.usgs.gov/products/mcd12q1v006/). The mean annual rates of mortality were from Anderegg et al. (2022)[11], and no new mortality data were produced. The US

boundary was from DATA.GOV (https://data.gov/). The data produced in this study are available from figshare[48] (doi:10.6084/m9.figshare.23730507): https://figshare.com/s/ace0046a5200b4451e82

CODE AVAILABILITY

All analysis was done in the open-source software R. The code is available from figshare[48] (doi:10.6084/m9.figshare.23730507): https://figshare.com/s/ace0046a5200b4451e82

Methods-only references

35. Robinson, N. P. *et al.* Terrestrial primary production for the conterminous United States derived from Landsat 30 m and MODIS 250 m. *Remote Sensing in Ecology and Conservation* **4**, 264–280 (2018).
36. Liang, S. *et al.* The Global Land Surface Satellite (GLASS) Product Suite. *Bulletin of the American Meteorological Society* **102**, E323–E337 (2021).
37. Zheng, Y. *et al.* Improved estimate of global gross primary production for reproducing its long-term variation, 1982–2017. *Earth System Science Data* **12**, 2725–2746 (2020).
38. Wang, S., Zhang, Y., Ju, W., Qiu, B. & Zhang, Z. Tracking the seasonal and inter-annual variations of global gross primary production during last four decades using satellite near-infrared reflectance data. *The Science of The Total Environment* **755**, 142569 (2020).
39. Wells, N., Goddard, S. & Hayes, M. J. A Self-Calibrating Palmer Drought Severity Index. *Journal of Climate* **17**, 2335–2351 (2004).
40. Abatzoglou, J. T., Dobrowski, S. Z., Parks, S. A. & Hegewisch, K. C. TerraClimate, a high-resolution global dataset of monthly climate and climatic water balance from 1958–2015. *Sci Data* **5**, 170191 (2018).
41. van der Schrier, G., Barichivich, J., Briffa, K. R. & Jones, P. D. A scPDSI-based global data set of dry and wet spells for 1901–2009. *Journal of Geophysical Research: Atmospheres* **118**, 4025–4048 (2013).
42. Aitken, A. C. On Least Squares and Linear Combination of Observations. *Proceedings of the Royal Society of Edinburgh* **55**, 42–48 (1936).
43. Breiman, L. Random Forests. *Machine Learning* **45**, 5–32 (2001).

44. Cao, S. *et al.* Spatiotemporally consistent global dataset of the GIMMS Leaf Area Index (GIMMS LAI4g) from 1982 to 2020. *Earth System Science Data Discussions* 1–31 (2023) doi:10.5194/essd-2023-68.

45. Cheng, W. *et al.* Global monthly gridded atmospheric carbon dioxide concentrations under the historical and future scenarios. *Sci Data* **9**, 83 (2022).

46. Qin, Y. *et al.* Agricultural risks from changing snowmelt. *Nat. Clim. Chang.* **10**, 459–465 (2020).

47. Stocker, B. D. *et al.* Drought impacts on terrestrial primary production underestimated by satellite monitoring. *Nat. Geosci.* **12**, 264–270 (2019).

48. Liu, M. *et al*. Forest sensitivity change in response to disturbances. figshare. Dataset. (2023) doi:10.6084/m9.figshare.23730507.

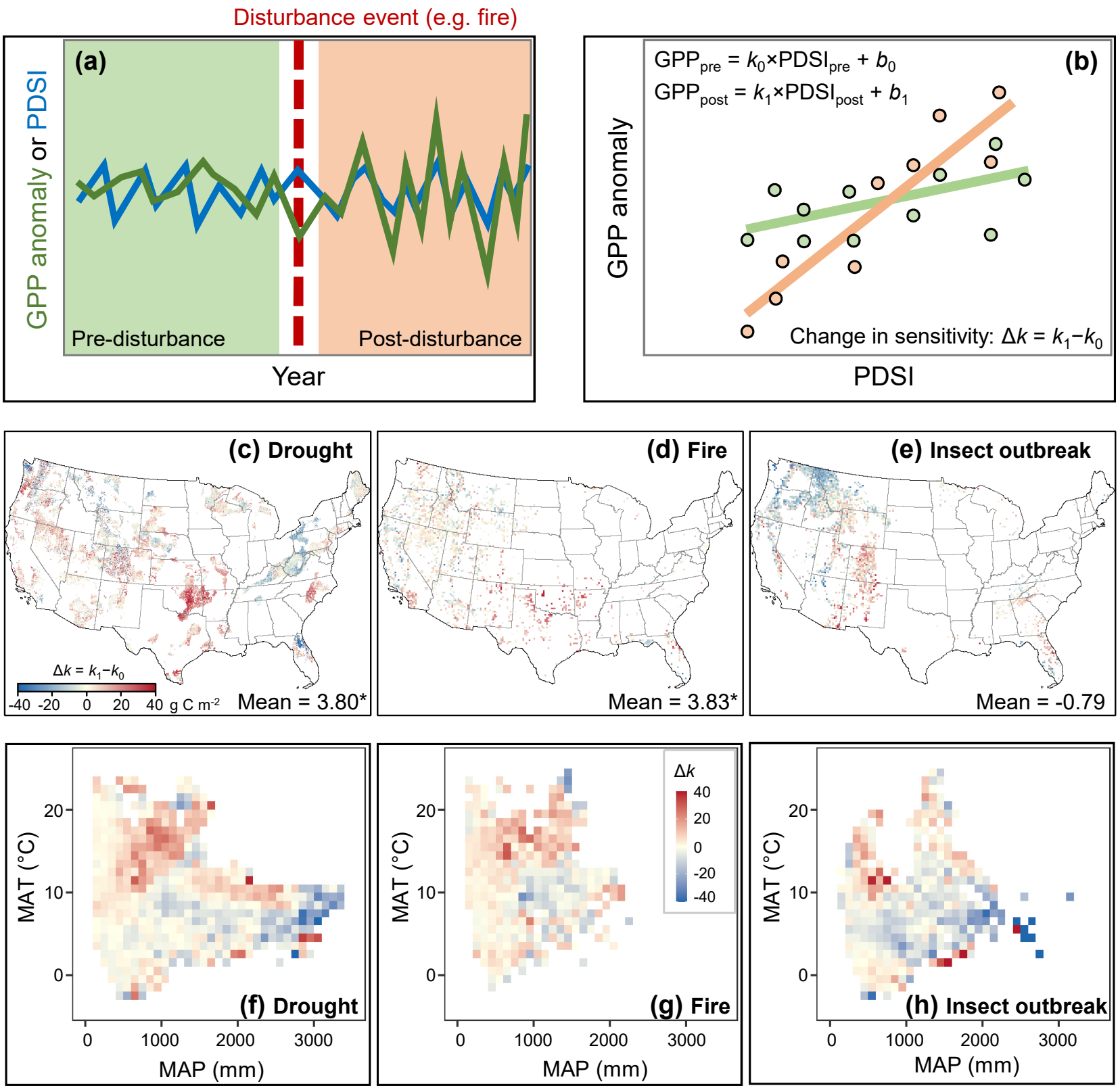
Disturbance event (e.g. fire)
(a)
GPP anomaly or PDSI
Pre-disturbance
Post-disturbance
Year
(b)
$GPP_{pre} = k_0 \times PDSI_{pre} + b_0$
$GPP_{post} = k_1 \times PDSI_{post} + b_1$
GPP anomaly
Change in sensitivity: $\Delta k = k_1 - k_0$
PDSI
(c) Drought
$\Delta k = k_1 - k_0$
-40 -20 0 20 40 g C m^{-2}
Mean = 3.80*
(d) Fire
Mean = 3.83*
(e) Insect outbreak
Mean = -0.79
MAT (°C)
MAP (mm)
(f) Drought
(g) Fire
(h) Insect outbreak
Δk
40
20
0
-20
-40

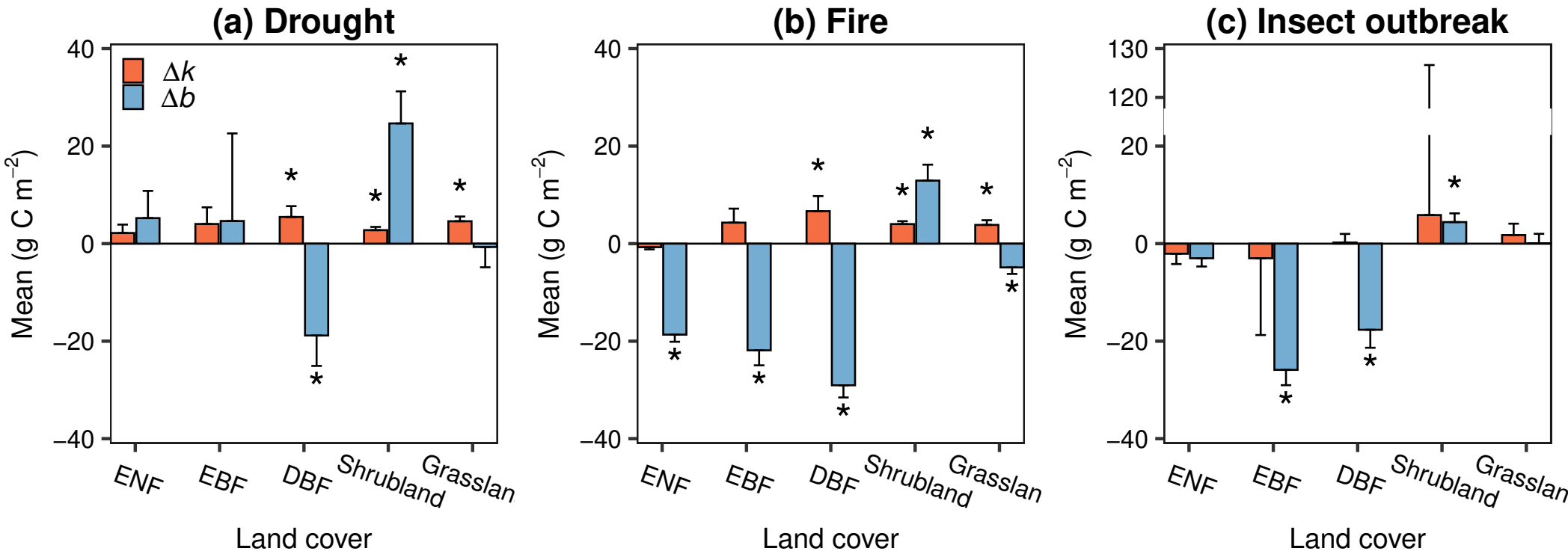
(a) Drought
(b) Fire
(c) Insect outbreak
Δk
Δb
Mean (g C m−2)
Land cover
ENF
EBF
DBF
Shrubland
Grasslan
40
20
0
−20
−40
130
120
*

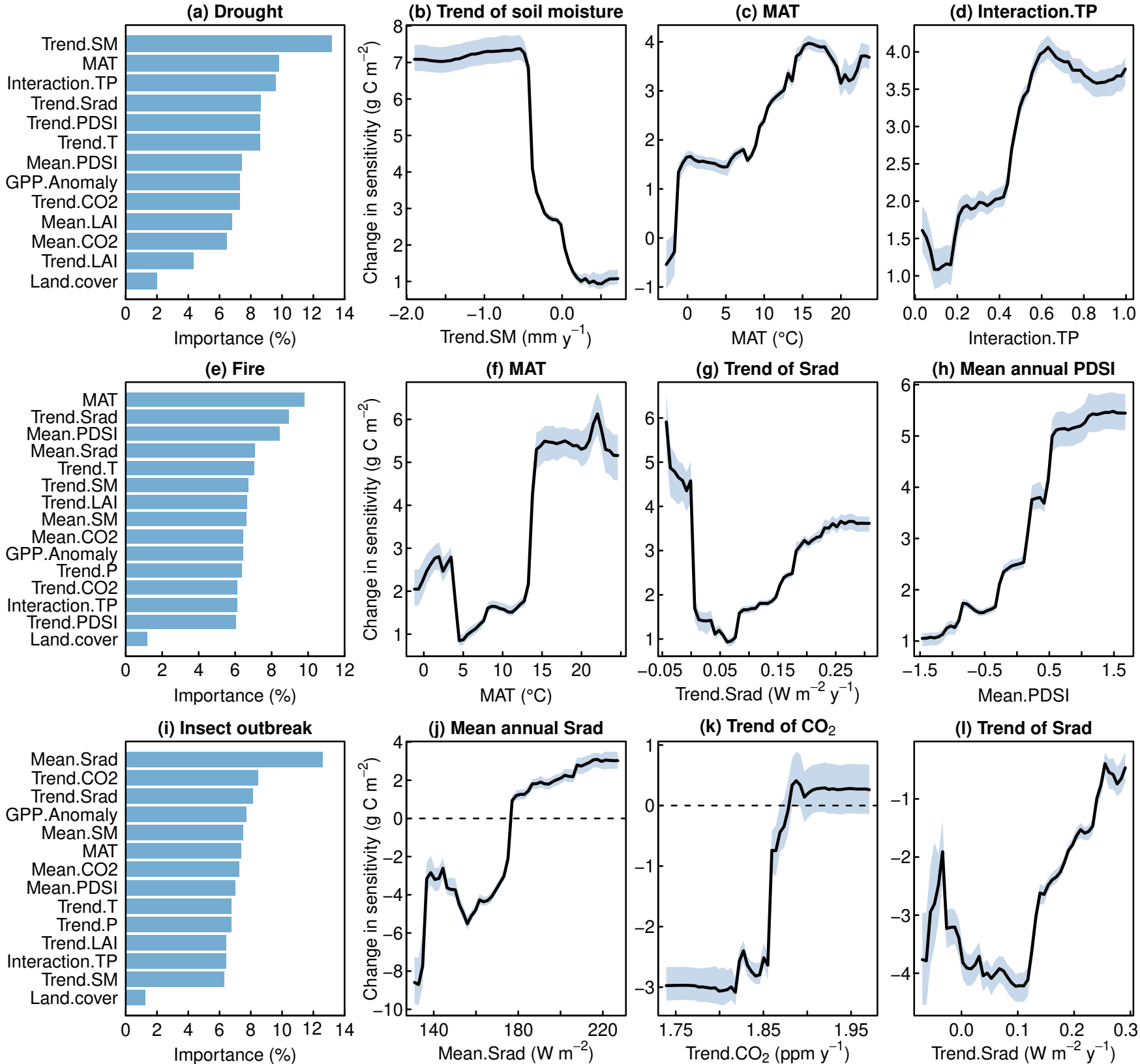
(a) Drought
Trend.SM
MAT
Interaction.TP
Trend.Srad
Trend.PDSI
Trend.T
Mean.PDSI
GPP.Anomaly
Trend.CO2
Mean.LAI
Mean.CO2
Trend.LAI
Land.cover
0 2 4 6 8 10 12 14
Importance (%)
(b) Trend of soil moisture
Change in sensitivity (g C m−2)
1 2 3 4 5 6 7 8
−2.0 −1.0 0.0
Trend.SM (mm y−1)
(c) MAT
−1 0 1 2 3 4
0 5 10 15 20
MAT (°C)
(d) Interaction.TP
1.0 1.5 2.0 2.5 3.0 3.5 4.0
0.0 0.2 0.4 0.6 0.8 1.0
Interaction.TP
(e) Fire
MAT
Trend.Srad
Mean.PDSI
Mean.Srad
Trend.T
Trend.SM
Trend.LAI
Mean.SM
Mean.CO2
GPP.Anomaly
Trend.P
Trend.CO2
Interaction.TP
Trend.PDSI
Land.cover
0 2 4 6 8 10 12
Importance (%)
(f) MAT
Change in sensitivity (g C m−2)
1 2 3 4 5 6
0 5 10 15 20
MAT (°C)
(g) Trend of Srad
1 2 3 4 5 6
−0.05 0.05 0.15 0.25
Trend.Srad (W m−2 y−1)
(h) Mean annual PDSI
1 2 3 4 5 6
−1.5 −0.5 0.5 1.5
Mean.PDSI
(i) Insect outbreak
Mean.Srad
Trend.CO2
Trend.Srad
GPP.Anomaly
Mean.SM
MAT
Mean.CO2
Mean.PDSI
Trend.T
Trend.P
Trend.LAI
Interaction.TP
Trend.SM
Land.cover
0 2 4 6 8 10 12 14
Importance (%)
(j) Mean annual Srad
Change in sensitivity (g C m−2)
−10 −8 −6 −4 −2 0 2 4
140 180 220
Mean.Srad (W m−2)
(k) Trend of CO2
−3 −2 −1 0 1
1.75 1.85 1.95
Trend.CO2 (ppm y−1)
(l) Trend of Srad
−4 −3 −2 −1
0.0 0.1 0.2 0.3
Trend.Srad (W m−2 y−1)

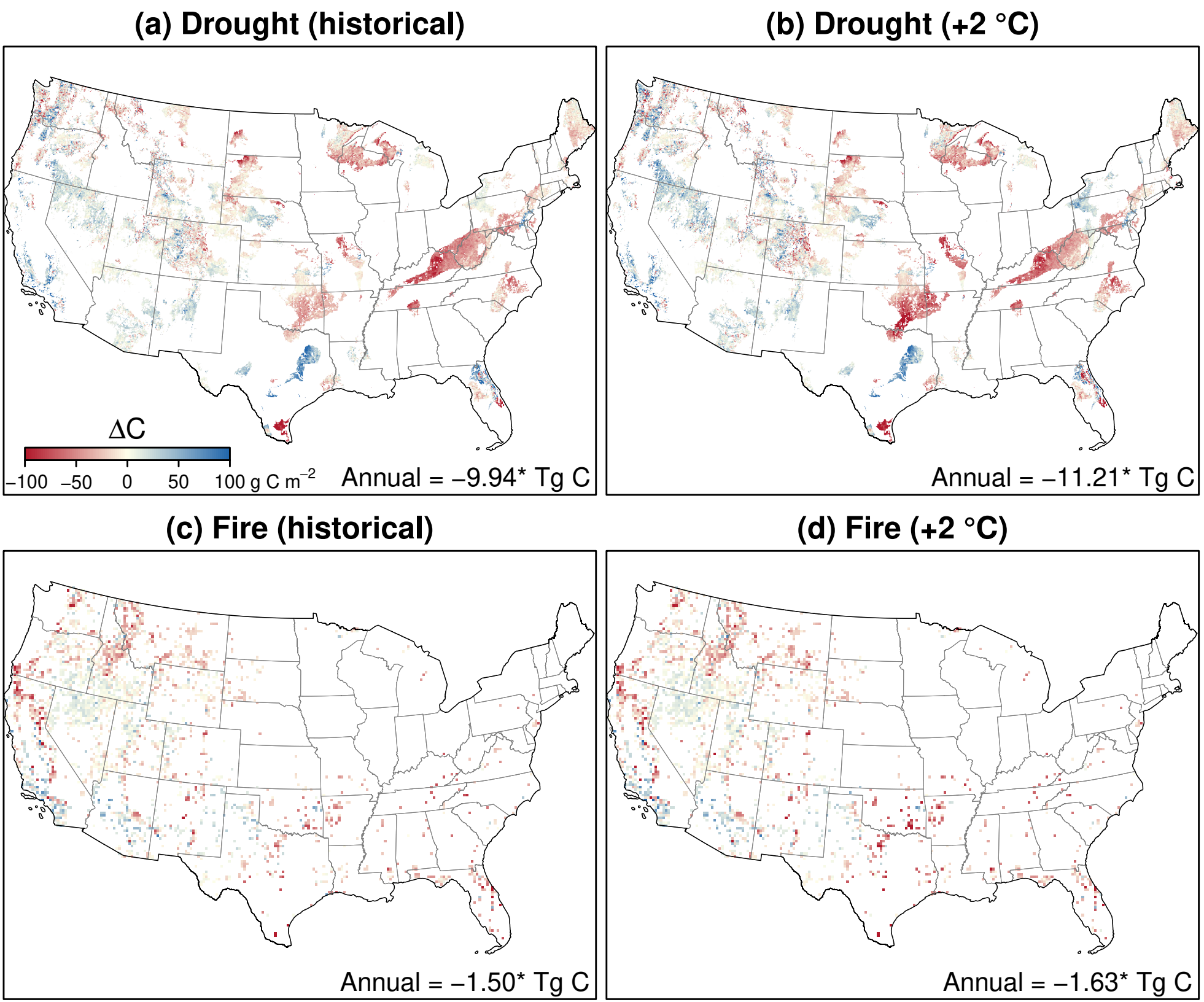
(a) Drought (historical)
(b) Drought (+2 °C)
(c) Fire (historical)
(d) Fire (+2 °C)
ΔC
−100 −50 0 50 100 g C m−2
Annual = −9.94* Tg C
Annual = −11.21* Tg C
Annual = −1.50* Tg C
Annual = −1.63* Tg C

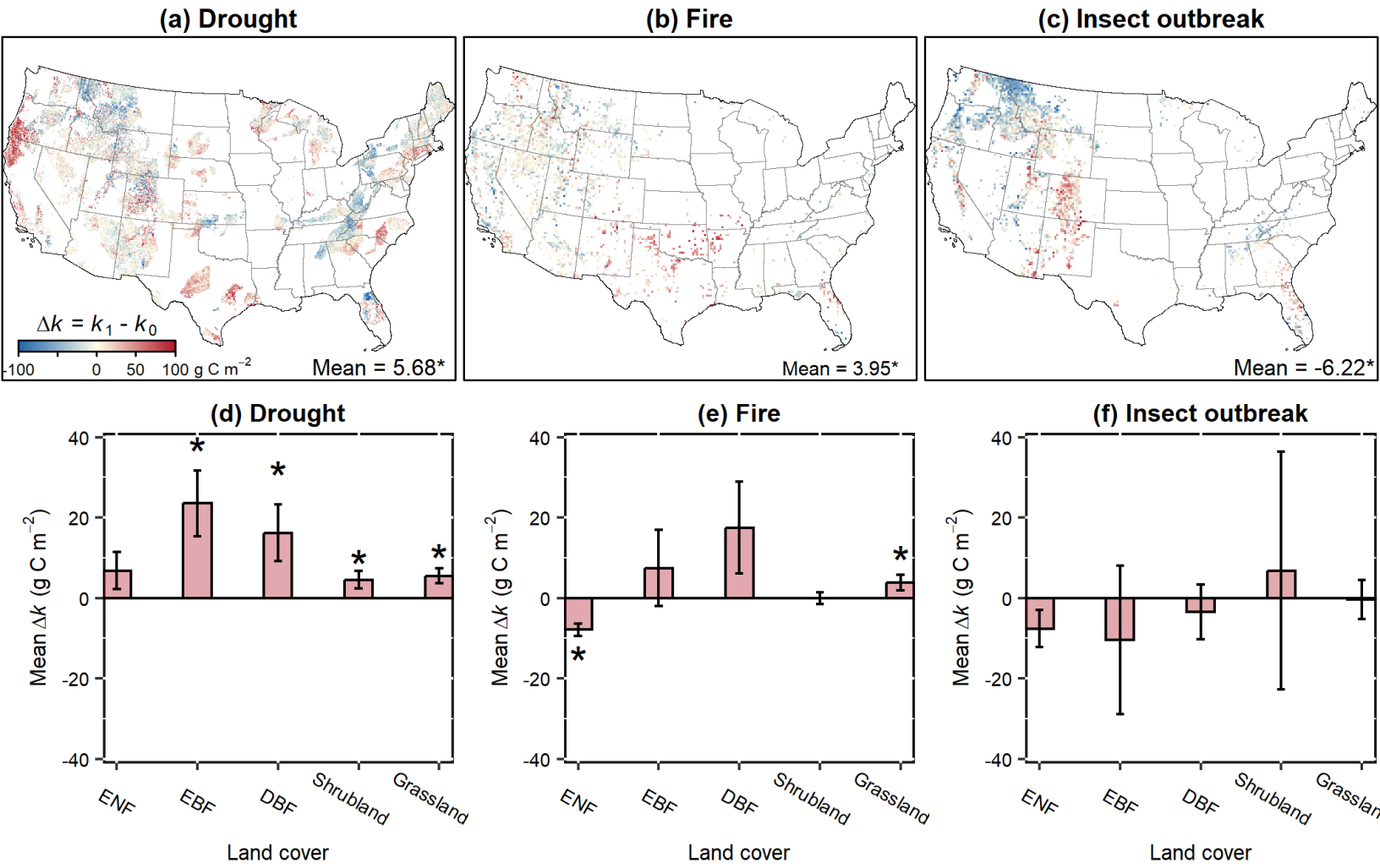
(a) Drought
(b) Fire
(c) Insect outbreak
Δk = k1 - k0
-100
0
50
100 g C m−2
Mean = 5.68*
Mean = 3.95*
Mean = -6.22*
(d) Drought
(e) Fire
(f) Insect outbreak
Mean Δk (g C m−2)
40
20
0
-20
-40
ENF
EBF
DBF
Shrubland
Grassland
Land cover

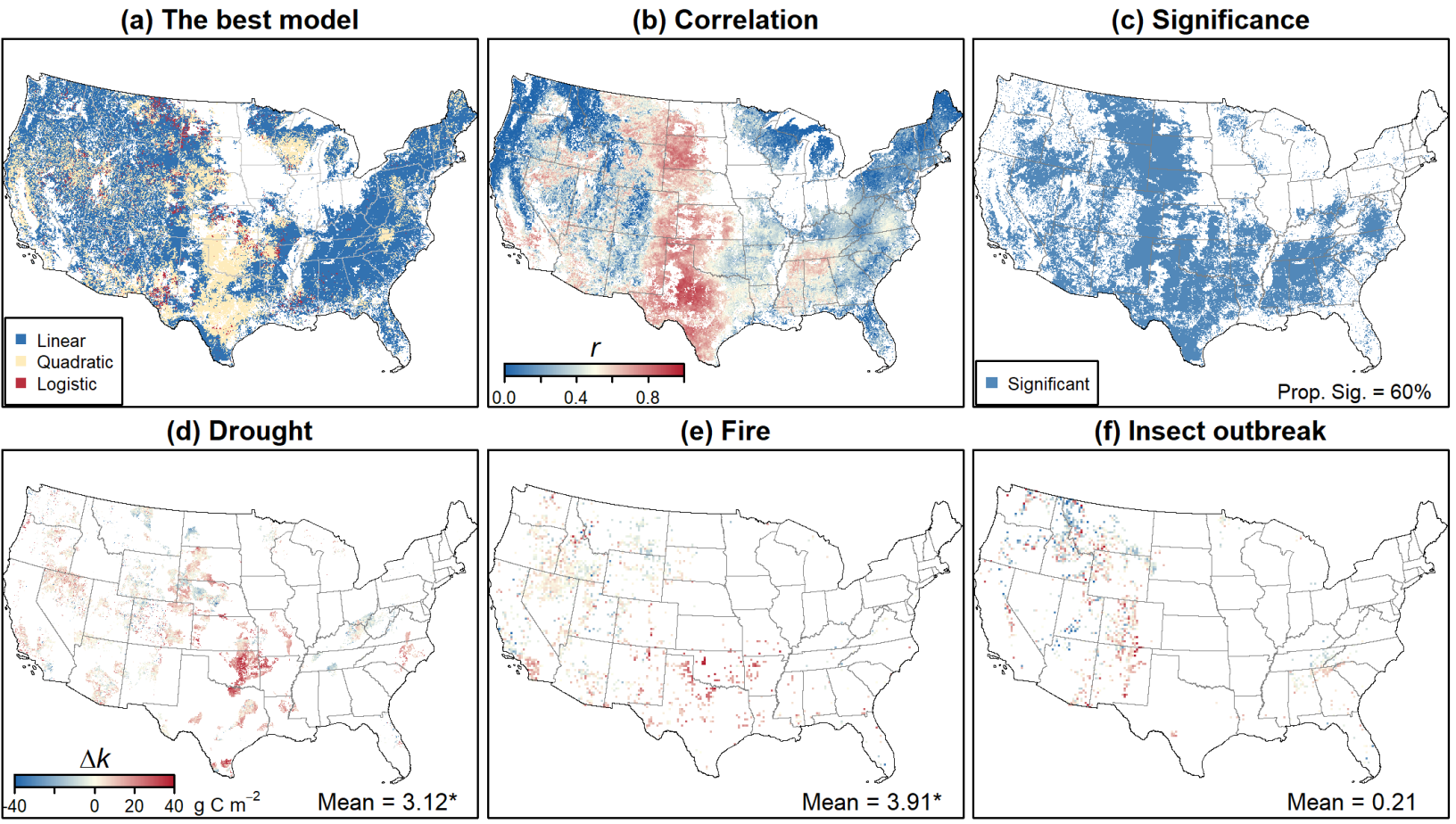
(a) The best model
Linear
Quadratic
Logistic
(b) Correlation
r
0.0
0.4
0.8
(c) Significance
Significant
Prop. Sig. = 60%
(d) Drought
Δk
-40
0
20
40
g C m−2
Mean = 3.12*
(e) Fire
Mean = 3.91*
(f) Insect outbreak
Mean = 0.21

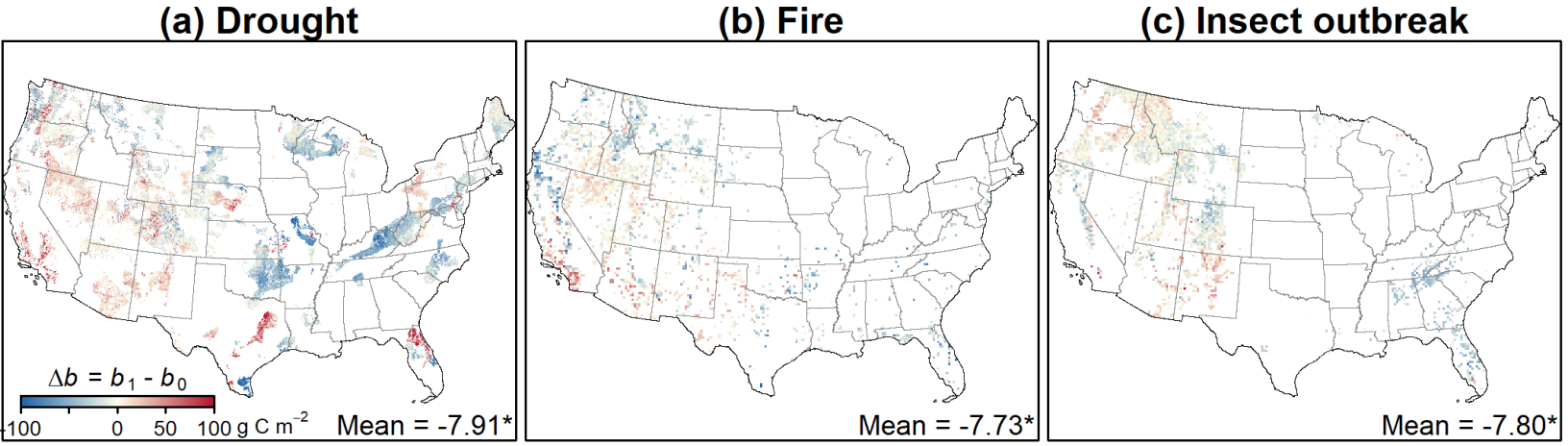
(a) Drought
(b) Fire
(c) Insect outbreak
Δb = b1 - b0
-100
0
50
100 g C m-2
Mean = -7.91*
Mean = -7.73*
Mean = -7.80*

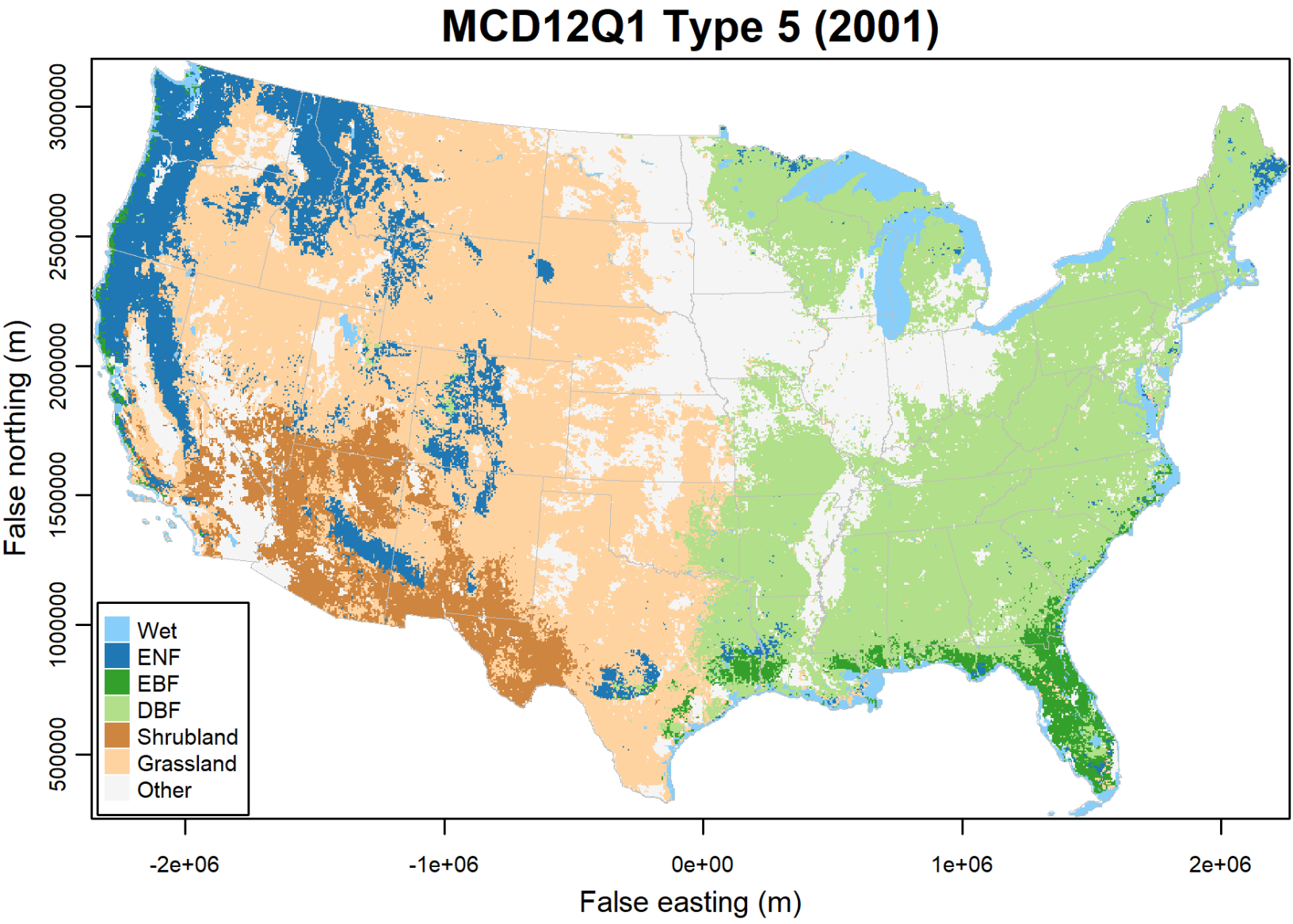
MCD12Q1 Type 5 (2001)
False northing (m)
3000000
2500000
2000000
1500000
1000000
500000
Wet
ENF
EBF
DBF
Shrubland
Grassland
Other
-2e+06
-1e+06
0e+00
1e+06
2e+06
False easting (m)

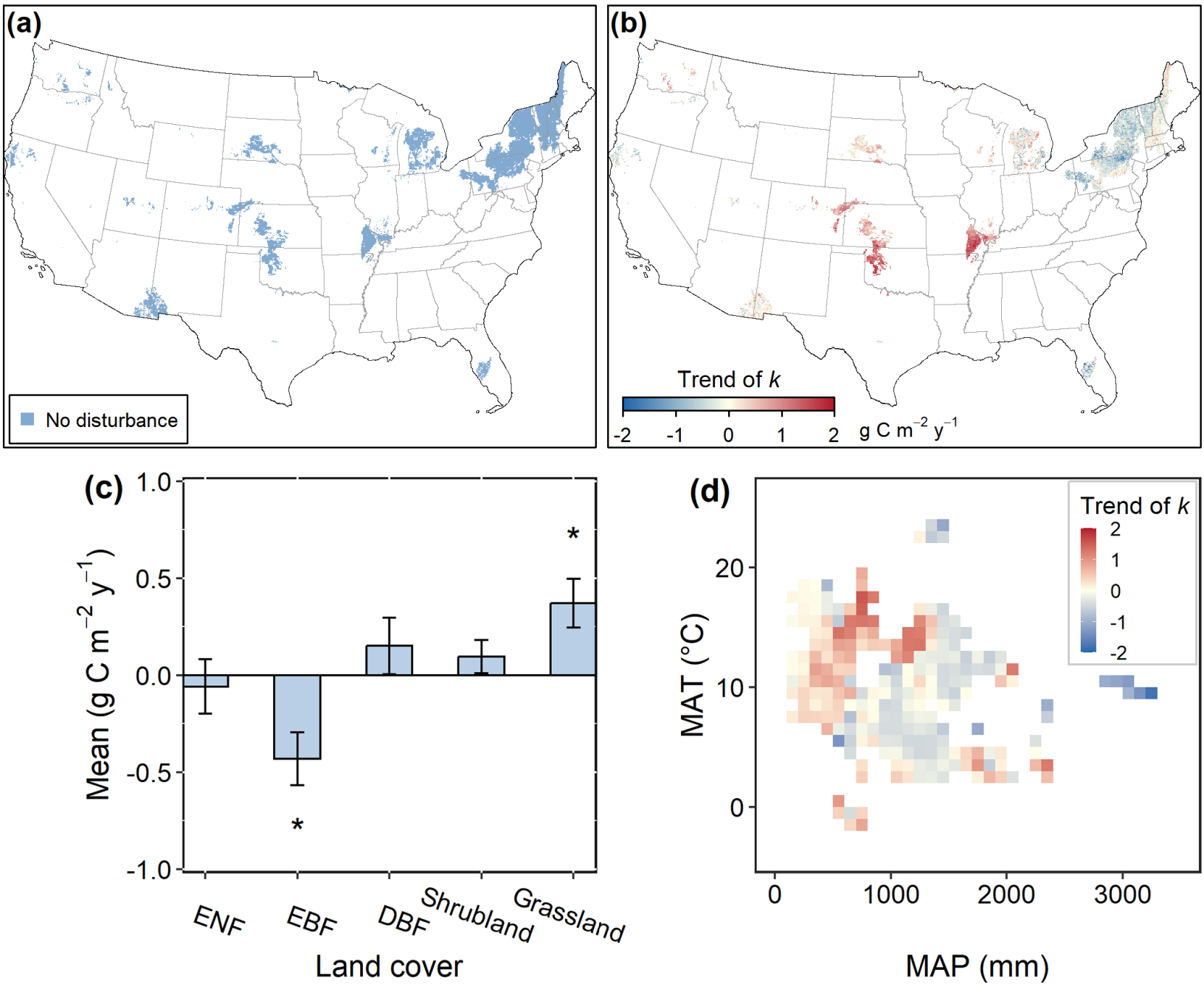
(a)
No disturbance
(b)
Trend of k
-2
-1
0
1
2
g C m−2 y−1
(c)
Mean (g C m−2 y−1)
1.0
0.5
0.0
-0.5
-1.0
*
*
ENF
EBF
DBF
Shrubland
Grassland
Land cover
(d)
Trend of k
2
1
0
-1
-2
MAT (°C)
20
10
0
0
1000
2000
3000
MAP (mm)

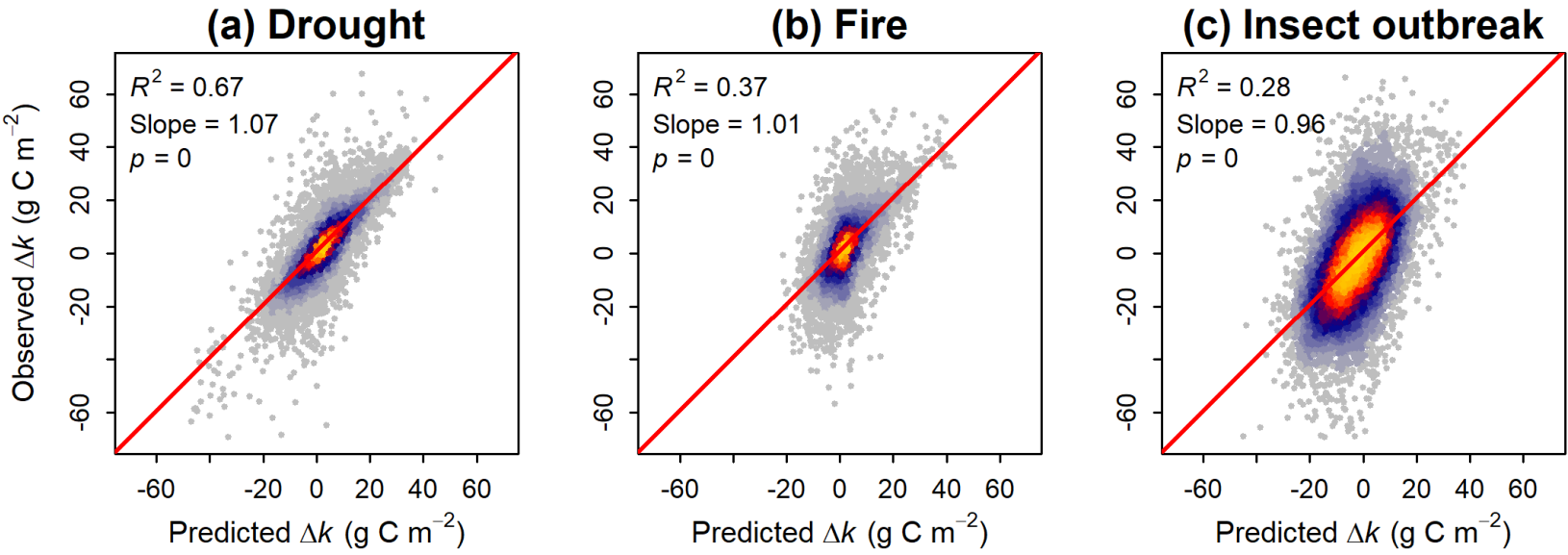
(a) Drought
(b) Fire
(c) Insect outbreak
R^2 = 0.67
Slope = 1.07
p = 0
R^2 = 0.37
Slope = 1.01
p = 0
R^2 = 0.28
Slope = 0.96
p = 0
Observed Δk (g C m^{-2})
Predicted Δk (g C m^{-2})
-60
-20
0
20
40
60

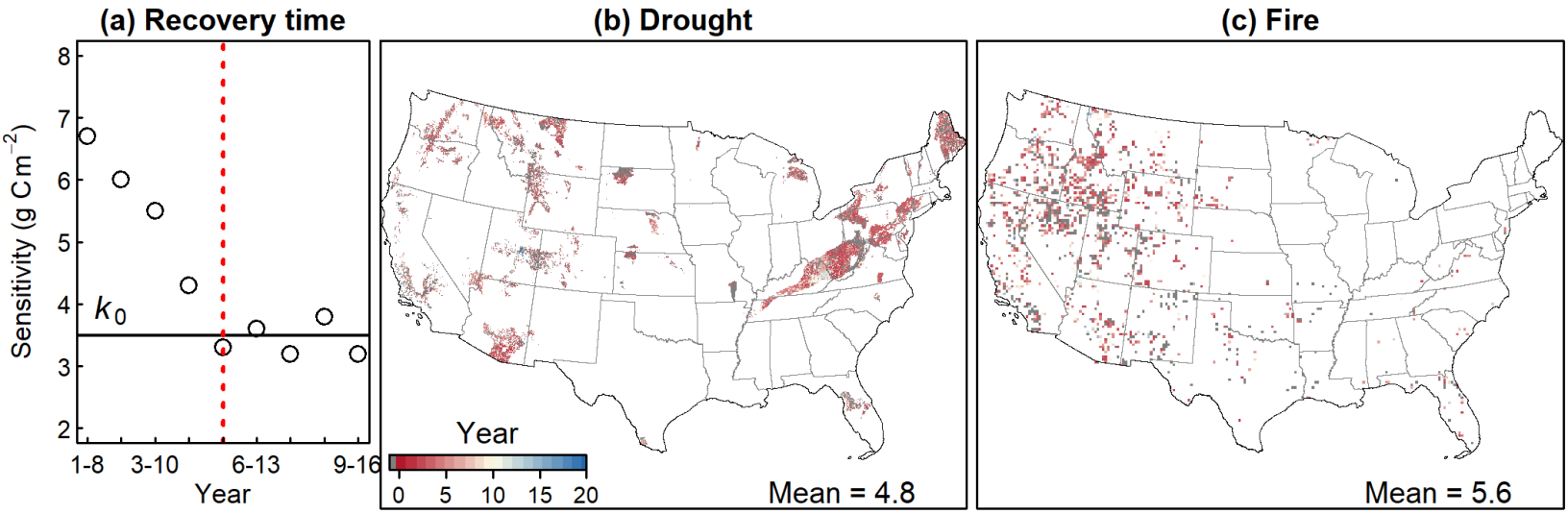
(a) Recovery time
(b) Drought
(c) Fire
Sensitivity (g C m^{-2})
8
7
6
5
4
3
2
k_0
1-8
3-10
6-13
9-16
Year
Year
0
5
10
15
20
Mean = 4.8
Mean = 5.6

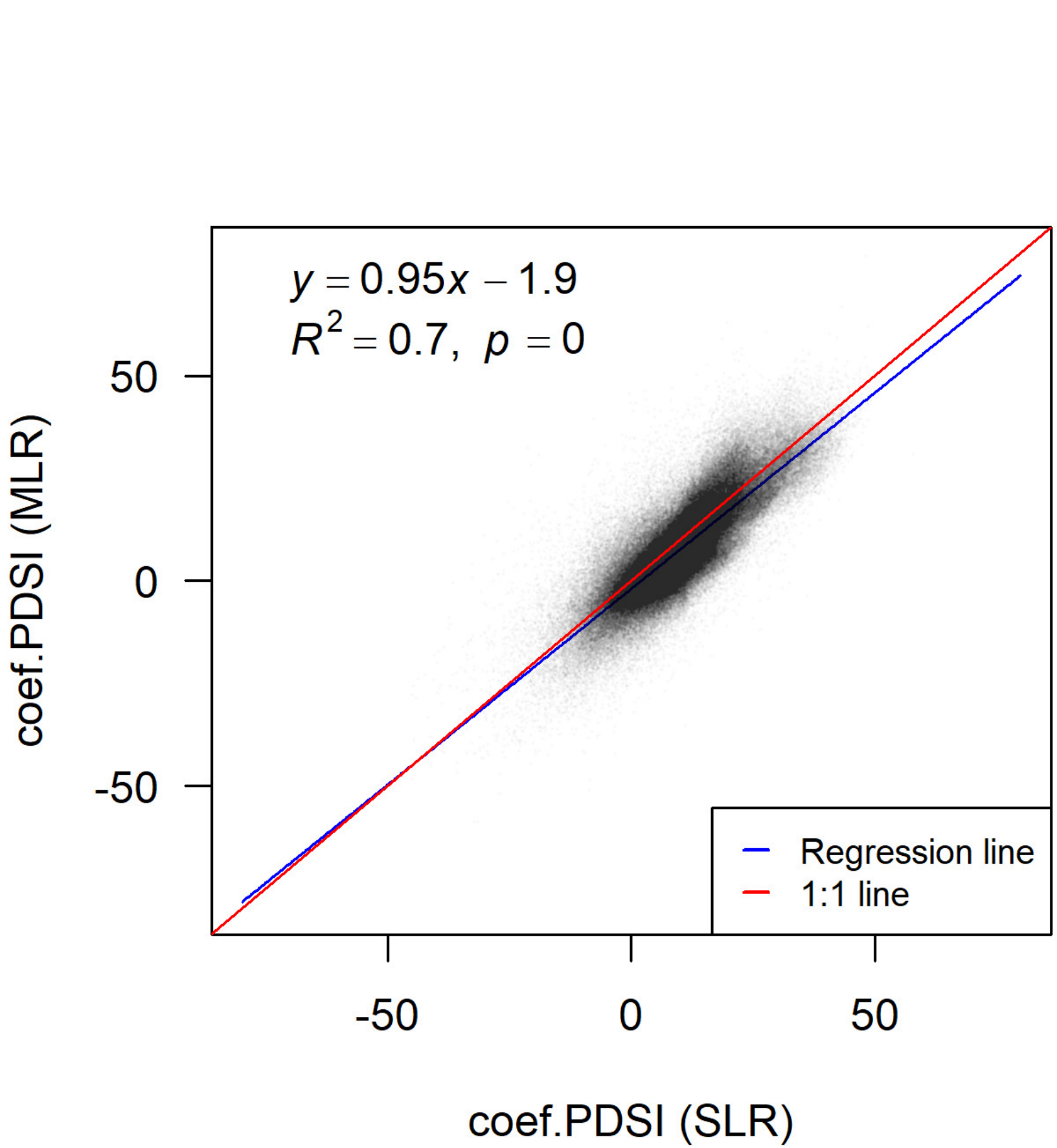
$y = 0.95x - 1.9$
$R^2 = 0.7,\ p = 0$
50
0
-50
coef.PDSI (MLR)
-50
0
50
coef.PDSI (SLR)
Regression line
1:1 line

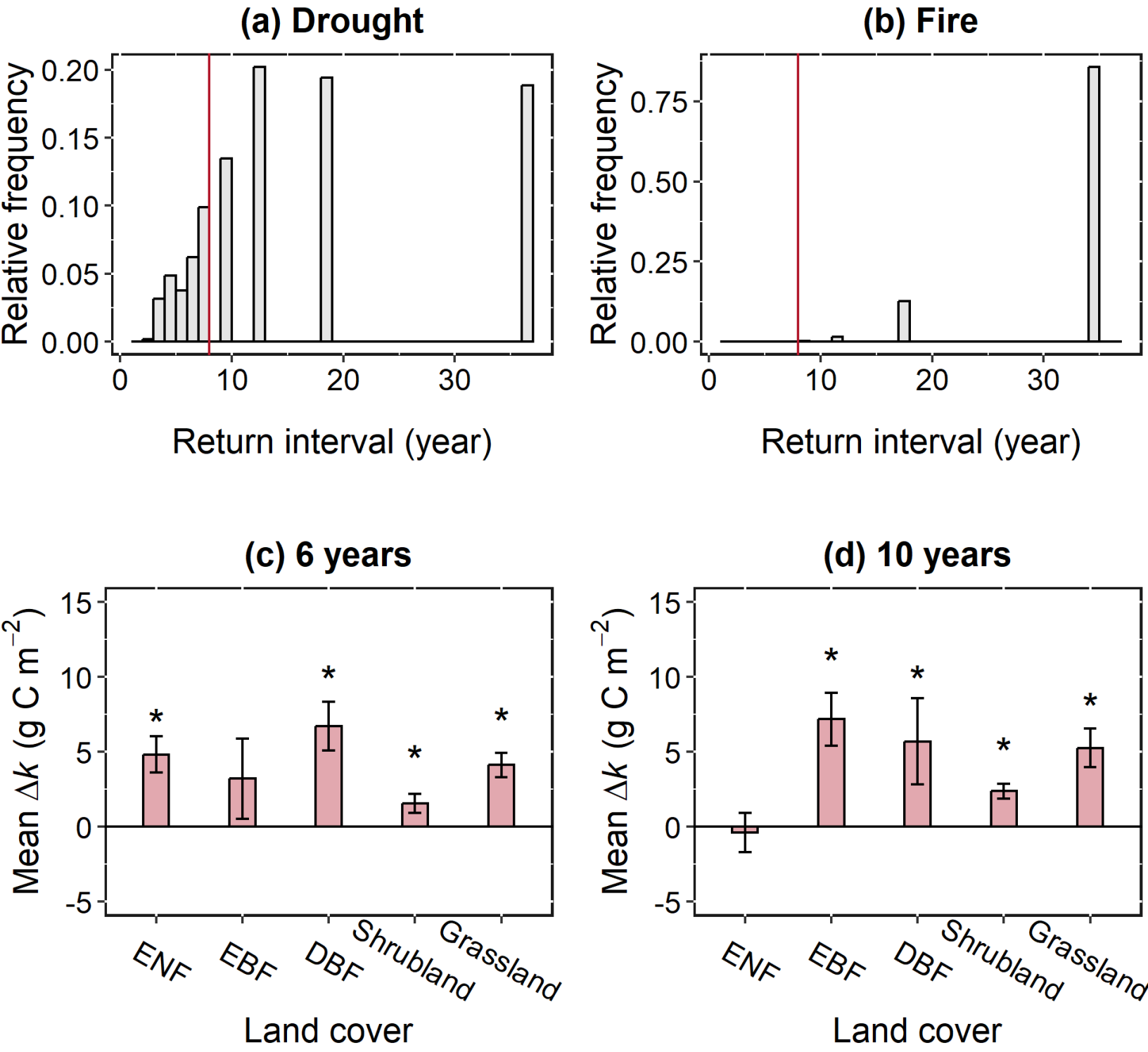
(a) Drought
Relative frequency
0.20
0.15
0.10
0.05
0.00
0
10
20
30
Return interval (year)
(b) Fire
Relative frequency
0.75
0.50
0.25
0.00
0
10
20
30
Return interval (year)
(c) 6 years
Mean Δk (g C m−2)
15
10
5
0
-5
*
ENF
EBF
DBF
Shrubland
Grassland
Land cover
(d) 10 years
Mean Δk (g C m−2)
15
10
5
0
-5
*
ENF
EBF
DBF
Shrubland
Grassland
Land cover

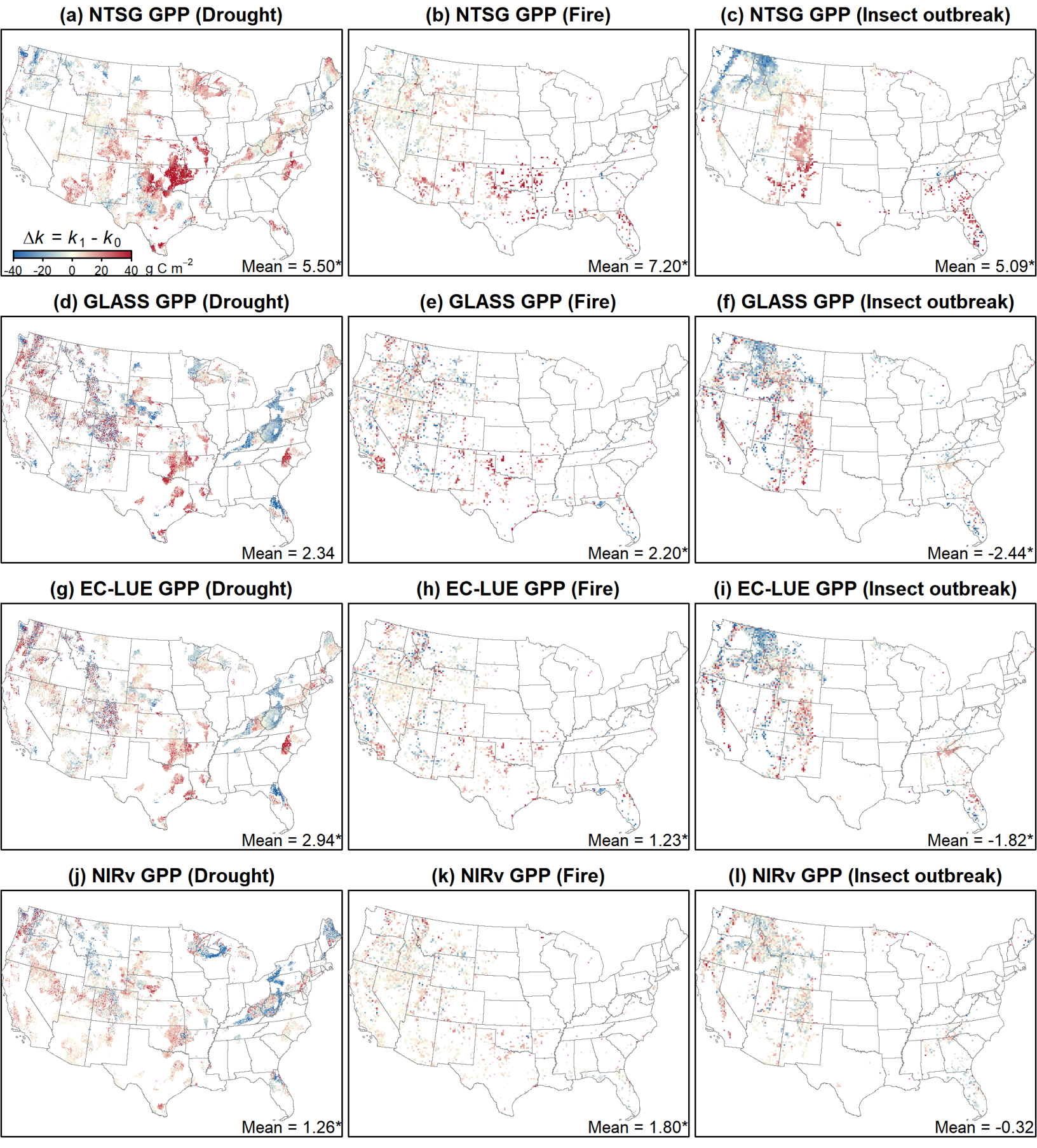
(a) NTSG GPP (Drought)
(b) NTSG GPP (Fire)
(c) NTSG GPP (Insect outbreak)
Δk = k1 - k0
-40 -20 0 20 40 g C m-2
Mean = 5.50*
Mean = 7.20*
Mean = 5.09*
(d) GLASS GPP (Drought)
(e) GLASS GPP (Fire)
(f) GLASS GPP (Insect outbreak)
Mean = 2.34
Mean = 2.20*
Mean = -2.44*
(g) EC-LUE GPP (Drought)
(h) EC-LUE GPP (Fire)
(i) EC-LUE GPP (Insect outbreak)
Mean = 2.94*
Mean = 1.23*
Mean = -1.82*
(j) NIRv GPP (Drought)
(k) NIRv GPP (Fire)
(l) NIRv GPP (Insect outbreak)
Mean = 1.26*
Mean = 1.80*
Mean = -0.32